Electronic Supplementary Material (ESI) for Chemical Communications.

Supporting Information

Self-assembly of small-molecule fumaramides allows transmembrane chloride channel formation

Arundhati Roy, Amitosh Gautam, Javid Ahmad Malla, Sohini Sarkar, Arnab Mukherjee, and Pinaki Talukdar*

Department of Chemistry, Indian Institute of Science Education and Research Pune, India. Fax: +91 20 2589 9790; Tel: +91 20 2590 8001

E-mail: ptalukdar@iiserpune.ac.in

Table of contents

I. General Methods and Physical Measurements

All chemical reactions were performed under the nitrogen atmosphere. All the reagents used for synthesis were purchased from commercial sources and used without further purification. Solvents were purchased as dry from commercial sources or dried by standard methods before using. Thin layer chromatography (TLC) was carried out with silica gel 60-F_{254} plates and column chromatography was performed over silica gel (100-200 mesh) acquired from commercial suppliers and accompanied with UV-detector (λ = 365 nm, 254 nm). Egg yolk phosphatidylcholine (EYPC) lipid was procured as a solution in chloroform (25 mg/mL). HEPES buffer, HPTS dye, lucigenin dye, Triton X-100, NaOH and inorganic salts were obtained as molecular biology grade. Gel-permeation chromatography was performed on a column of Sephadex G-50 in buffer containing salt solution or only salt solution, as per requirement. Large unilamellar vesicles (LUVs) were prepared by using mini extruder, equipped with a polycarbonate membrane of 100 nm (in case of HPTS Assay) or 200 nm (in case of Lucigenin Assay) pore size.

The ^{1}H and ^{13}C spectra were recorded on 400 MHz for ^{1}H or 100 MHz for ^{13}C spectrometers using either residual solvent signals as an internal reference on the δ scale (DMSO-d_6 δ_H 2.50 ppm, MeOH-d_4 δ_H 3.31 ppm, $CDCl_3$ δ_H 7.26 ppm and DMSO-d_6 δ_C 39.52 ppm, MeOH-d_4 δ_C 49.00 ppm, $CDCl_3$ δ_C 77.16 ppm). The chemical shifts (δ) are reported in ppm and coupling constants (J) are presented as Hz. The following abbreviations are used for NMR signal processing: s (singlet), d (doublet) m (multiplet), dd (doublet of doublet), td (triplet of doublet). High-resolution mass spectra (HRMS) were obtained from ESI-TOF MS spectrometer. Steady State fluorescence experiments were carried out in a micro fluorescence cuvette on a Fluorescence instrument equipped with an injector port and a magnetic stirrer. Infrared (IR) spectra were obtained using FT-IR spectrophotometer as KBr disc and reported in cm^{-1}. Melting points of all solid compounds were measured using a Melting point apparatus using open glass capillary and values are uncorrected. The pH of the HEPES buffer solutions used for fluorescence experiment was adjusted as per requirement by NaOH using a pH-meter.

II. Synthesis

Synthesis of compound (*S*)-(1,4-dioxaspiro[4.5]decan-2-yl)methanamine 5c:

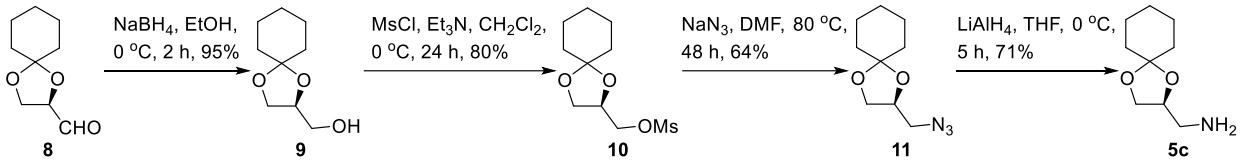

Scheme S1. Synthesis of compound **5c**.

At first compound **8** was prepared following a reported protocol.[S1] Compound **8** was then converted to **9** according to a reported procedure.[S2] Compound **9** was further mesylated following a reported protocol[S3] to give compound **10**.

Synthesis of compound 11: In a 50 mL round bottom flask, NaN_3 (850 mg) was added to a solution of **10** (2.7 g) in dry dimethylformamide (DMF) (15 mL) at room temperature and the reaction was stirred at 80 °C for 48 h. After that the resultant mixture was extracted with ethyl acetate. The organic layer was concentrated under *vacuo* and subsequently purified by flash column chromatography with chloroform as eluent to give **11** (1.3 g, 64%). Obtained compound was directly used for next step to synthesize compound **5c**.

Synthesis of compound 5c: In a 50 mL round bottom flask, compound **11** (500 mg, 2.5 mmol) was taken in dry THF (15 mL) under nitrogen atmosphere and cooled down to at 0 °C. Then $LiAlH_4$ (144 mg) was added portionwise. Ice bath was removed and the resultant mixture was stirred at room temperature for 5h. After that the reaction was cooled to 0 °C and ethyl acetate was added slowly followed by the addition of saturated Na_2SO_4 to quench $LiAlH_4$. White precipitate was formed which was filtered off and filtrate was extracted with ethyl acetate and dried over Na_2SO_4 and concentrated under reduced pressure to obtain compound **5c** (410 mg) as transparent liquid. (308 mg, 71%). Obtained 1H-NMR data was matching with reported product.[S4]

General procedure for synthesizing fumaramide derivatives (1a – 5a): In a 25 mL round bottom flask, a solution of amine **1c** – **5c** (3.92 mmol) and Et_3N (364 µL, 2.61 mmol) in CH_3CN (4 mL) were taken and cooled to 0 °C. A solution of fumaryl chloride (200 mg, 133 µL, 1.30 mmol) in CH_3CN (2 mL) was added drop wise during a period of 1 h at same temperature. The reaction mixture was stirred for additional 1 h at room temperature. White precipitate was observed in the reaction mixture. After completion of reaction, solvent was removed under reduced pressure. The obtained residue was partially dissolved in EtOAc (2 × 100 mL) and transferred to a separatory funnel. The organic layer was washed first with water (2 × 100 mL) and then with brine (2 × 50 mL) solution. The organic layer was then evaporated under reduced pressure to obtain light brown to white solid, which was further purified by column chromatography over silica gel. Expected product was obtained as white solid with 53 – 95% yield.

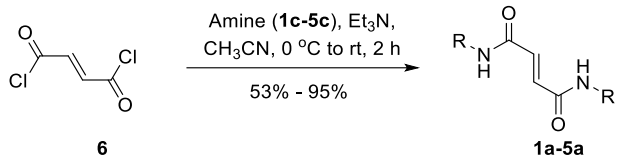

Scheme S2. General scheme for the synthesis of **1a-5a**.

Synthesis of *N*^{1}, *N*^{4}-dibutylfumaramide (1a):

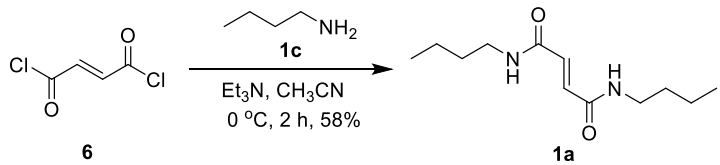

Scheme S3. Synthesis of compound **1a**.

Compound **1a** (170 mg, 58%) was obtained as white solid. **M.p.:** 270 – 271 °C; **IR (KBr):** ν/cm^{-1} 3286, 3070, 2947, 2857, 1632, 1545, 1457, 1343, 1192, 991; **^{1}H NMR (400 MHz, DMSO-d_6):** δ 8.34 (s, 2H), 6.79 (s, 2H), 3.14 (dd, J = 6.8 Hz, 6 Hz, 4H), 1.41 (m, 4H), 1.23 (m, 4H), 0.87 (t, J = 7.2 Hz, 6H); **^{13}C NMR (100 MHz, DMSO-d_6):** δ 163.4, 132.1, 38.0, 30.5, 19.0, 12.9; **HRMS (ESI):** Calc. for $C_{12}H_{23}N_2O_2$ $[M+H]^+$: 227.1759; Found: 227.1765.

Synthesis of *N*^{1}, *N*^{4}-dihexylfumaramide (2a):

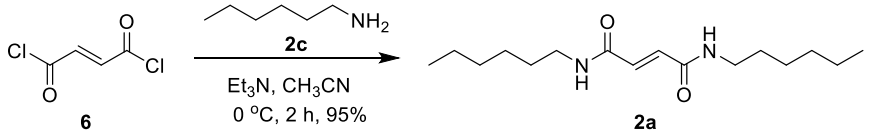

Scheme S4. Synthesis of compound **2a**.

Compound **2a** (350 mg, 95%) was obtained as white solid.[S5] **M.p.:** 210 – 211 °C; **IR (KBr):** ν/cm^{-1} 3290, 3067, 2944, 2850, 2746, 1631, 1543, 1458, 1327, 1190; **^{1}H NMR (400 MHz, MeOH-d_4):** δ 6.89 (s, 2H), 3.24 (t, J = 7.2 Hz, 4H), 1.54 (m, 4H), 1.33 (m, 12H), 0.91 (m, 6H); **^{13}C NMR (100 MHz, DMSO-d_6):** δ 163.2, 131.8, 38.1, 30.1, 28.1, 25.3, 21.1, 12.9; **HRMS (ESI):** Calc. for $C_{16}H_{31}N_2O_2$ $[M+H]^+$: 283.2385; Found: 283.2380.

Synthesis of *N*^{1}, *N*^{4}-dicyclohexylfumaramide (3a):

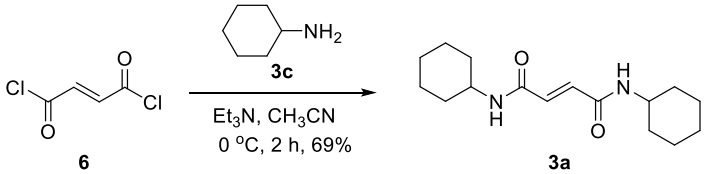

Scheme S5. Synthesis of compound **3a**.

Compound **3a** (250 mg, 69%) was obtained as white solid. All data was matching with reported data.[S6] **M.p.:** > 300 °C; **IR (KBr):** ν/cm^{-1} 3286, 3078, 2926, 1636, 1545, 1445, 1345, 1181, 994; **^{1}H NMR (400 MHz, DMSO-d_6):** δ 7.90 (s, 2H), 6.80 (s, 2H), 3.65 (m, 2H), 1.55 (m, 10H), 1.16 (m, 10H); **^{13}C NMR (100 MHz, DMSO-d_6):** δ 162.6, 132.3, 47.3, 31.7, 24.7, 23.8; **HRMS (ESI):** Calc. for $C_{16}H_{27}N_2O_2$ $[M+H]^+$: 279.2072; Found: 279.2064.

Synthesis of *N*^{1},*N*^{4}-bis(((*S*)-2,2-dimethyl-1,3-dioxolan-4-yl)methyl)fumaramide (4a):

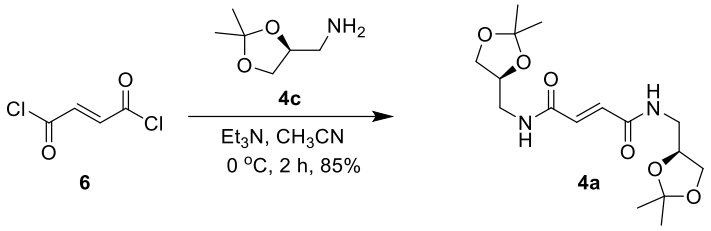

Scheme S6. Synthesis of compound **4a**.

The amine **4c** was synthesized according to reported protocol.[S7] Compound **4a** (380 mg, 85%) was obtained as colorless semi-solid. **M.p.:** 195 – 196 °C; **IR (KBr):** ν/cm^{-1} 3250, 3093, 2931, 1634, 1582, 1376, 1337, 1245, 1213, 1156; **^{1}H NMR (400 MHz, MeOH-*d*$_4$):** *δ* 6.91 (s, 2H), 4.19 (m, 2H), 4.02 (m, 2H), 3.65 (m, 2H), 3.36 (m, 4H), 1.36 (s, 6H), 1.31 (s, 6H); **^{13}C NMR (100 MHz, DMSO-*d*$_6$):** *δ* 163.9, 132.6, 108.4, 74.1, 66.5, 41.4, 26.7, 25.3; **HRMS (ESI):** Calc. for $C_{16}H_{26}N_2O_6Na$ [M+Na]$^+$: 365.1688; Found: 365.1694.

Synthesis of *N*^{1},*N*^{4}-bis(((*S*)-1,4-dioxaspiro[4.5]decan-2-yl)methyl)fumaramide (5a):

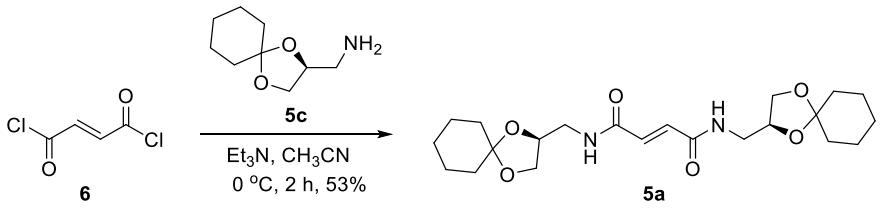

Scheme S7. Synthesis of compound **5a**.

Compound **5a** (290 mg, 53%) was obtained as white solid. **M.p.:** 290 – 291 °C; **IR (KBr):** ν/cm^{-1} 3532, 3295, 3083, 2941, 2854, 1644, 1548, 1446, 1348, 1263; **^{1}H NMR (400 MHz, DMSO-*d*$_6$):** *δ* 8.51 (t, *J* = 6 Hz, 2H), 6.85 (s, 2H), 4.06 (p, *J* = 6.0 Hz, 2H), 3.93 (d, *J* = 6.0 Hz, 2H), 3.57 (d, *J* = 6.0 Hz, 2H), 3.25 (t, *J* = 5.6 Hz, 4H), 1.32 (m, 20H); **^{13}C NMR (100 MHz, DMSO-*d*$_6$):** *δ* 163.9, 132.6, 108.8, 73.7, 66.2, 41.5, 36.1, 34.5, 24.6, 23.5, 23.4; **HRMS (ESI):** Calc. for $C_{22}H_{34}N_2O_6Na$ [M+Na]$^+$: 445.2314; Found: 445.2319.

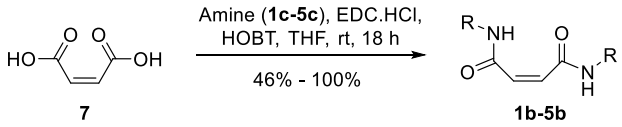

Scheme S8. General scheme for the synthesis of **1b-5b**.

General procedure for synthesizing maleamide derivatives (1b – 5b): In a 25 mL round bottom flask, maleic acid (200 mg, 1.72 mmol), amine **1c** – **5c** (4.13 mmol) and HOBT (632 mg, 4.13 mmol) were dissolved in THF (12 mL) and cooled to 0 °C. Then EDC·HCl (989 mg, 5.16 mmol) was added in portions to the above reaction mixture. The reaction mixture was stirred at room temperature for 18 h. After completion of reaction, THF was removed under reduced pressure and obtained residue was extracted with ethyl acetate (2 × 100 mL) and water (2 × 100 mL). Organic layer was washed with brine solution (2 × 50 mL) and then evaporated under vacuo to give light brown residue. Column chromatography was performed over silica gel to get the expected compound as either semi-solid or solid (colorless to white solid) with 46 – 100% yield.

Synthesis of N^1, N^4-dibutylmaleamide (1b):

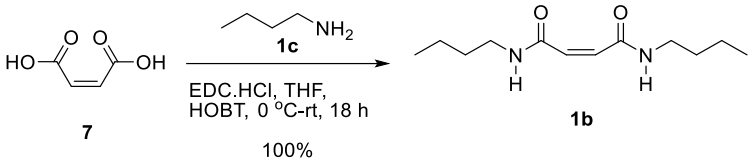

Scheme S9. Synthesis of compound **1b**.

Compound **1b** (173 mg, 100%) was obtained as colorless yellow semi-solid. All data was matching with reported data.[S8] **IR (KBr):** ν/cm^{-1} 3270, 3061, 2958, 2930, 2868, 1666, 1614, 1548, 1462, 1372; **^{1}H NMR (400 MHz, DMSO-d_6):** δ 9.20 (t, J = 5.6 Hz, 2H), 6.08 (s, 2H), 3.08 (m, 4H), 1.34 (m, 4H), 1.25 (m, 4H), 0.85 (t, J = 7.2 Hz, 6H); **^{13}C NMR (100 MHz, DMSO-d_6):** δ 164.4, 131.8, 38.3, 30.8, 19.6, 13.6; **HRMS (ESI):** Calc. for $C_{12}H_{23}N_2O_2$ $[M+H]^+$: 227.1759; Found: 227.1769.

Synthesis of N^1, N^4-dihexanoylmaleamide (2b):

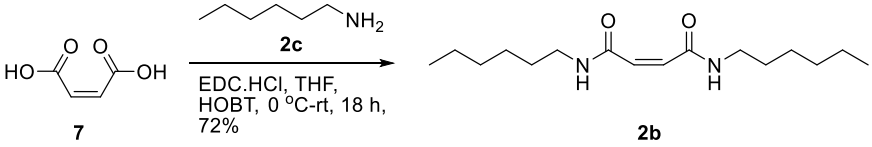

Scheme S10. Synthesis of compound **2b**.

Compound **2b** (350 mg, 72%) was obtained as colorless semi-solid. **IR (KBr):** ν/cm^{-1} 3281, 3063, 2926, 2860, 1666, 1615, 1549, 1461, 1371, 1265; **^{1}H NMR (400 MHz, DMSO-d_6):** δ 9.24 (t, J = 5.2 Hz, 2H), 6.08 (s, 2H), 3.08 (m, 4H), 1.38 (m, 4H), 1.25 (m, 12H), 0.83 (m, 6H); **^{13}C NMR (100 MHz, DMSO-d_6):** δ 164.4, 131.9, 38.7, 30.9, 28.7, 26.1, 22.0, 13.8; **HRMS (ESI):** Calc. for $C_{16}H_{31}N_2O_2$ $[M+H]^+$: 283.2385; Found: 283.2390.

Synthesis of N^1, N^4-dicyclohexylmaleamide (3b):

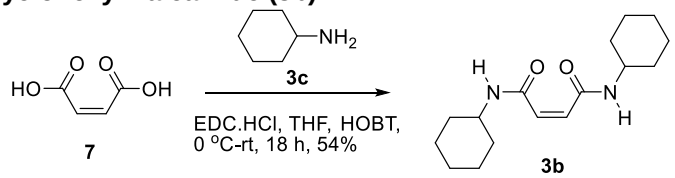

Scheme S11. Synthesis of compound **3b**.

Compound **3b** (260 mg, 54%) was obtained as white solid. **M.p.:** 132 – 133 °C; **IR (KBr):** ν/cm^{-1} 3270, 3070, 2932, 2843, 1613, 1531, 1444, 1337, 1245, 1093; **^{1}H NMR (400 MHz, MeOH-d_4):** δ 6.13 (s, 2H), 3.66 (m, 2H), 1.87 (dd, J = 2.8, 12.4 Hz, 4H), 1.74 (td, J = 3.6, 13.2 Hz, 4H), 1.62 (m, 2H), 1.22 (m, 10H); **^{13}C NMR (100 MHz, MeOH-d_4):** δ 166.1, 133.1, 49.8, 33.4, 26.6, 25.9; **HRMS (ESI):** Calc. for $C_{16}H_{27}N_2O_2$ $[M+H]^+$: 279.2072; Found: 279.2069.

Synthesis of *N*^{1},*N*^{4}-bis(((*S*)-2,2-dimethyl-1,3-dioxolan-4-yl)methyl)maleamide (4b):

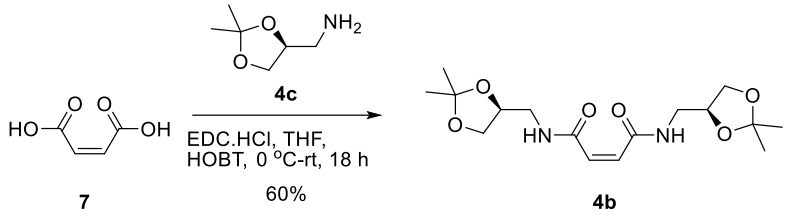

Scheme S12. Synthesis of compound **4b**.

Compound **4b** (349 mg) was obtained as colorless semi-solid with 60% yield. **IR (KBr):** ν/cm^{-1} 3217, 3059, 2985, 2935, 2882, 1668, 1618, 1547, 1451, 1375; **^{1}H NMR (400 MHz, CDCl$_3$):** *δ* 8.19 (s, 2H), 6.12 (s, 2H), 4.25 (m, 2H), 4.04 (m, 2H), 3.67 (m, 2H), 3.60 (m, 2H), 3.37 (m, 2H), 1.44 (s, 6H), 1.35 (m, 6H); **^{13}C NMR (100 MHz, CDCl$_3$):** *δ* 164.7, 132.3, 109.3, 74.0, 66.6, 41.7, 26.5, 25.0; **HRMS (ESI):** Calc. for $C_{16}H_{27}N_2O_6$ [M+H]$^+$: Calc. for 343.1864; Found: 343.1871.

Synthesis of *N*^{1},*N*^{4}-bis(((*S*)-1,4-dioxaspiro[4.5]decan-2-yl)methyl)maleamide (5b):

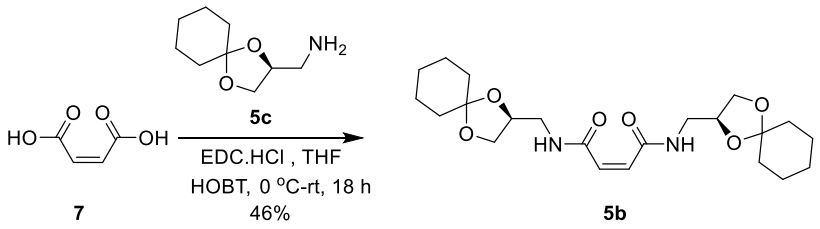

Scheme S13. Synthesis of compound **5b**.

Compound **5b** (333 mg, 46%) was obtained as colorless semi-solid. **IR (KBr):** ν/cm^{-1} 3279, 2933, 2858, 1669, 1618, 1548, 1441, 1366, 1222, 1163; **^{1}H NMR (400 MHz, DMSO-*d*$_6$/CDCl$_3$(1:1)):** *δ* 9.07 (t, *J* = 5.6 Hz, 2H), 6.15 (s, 2H), 4.08 (t, *J* = 5.6 Hz, 2H), 3.93 (t, *J* = 6 Hz, 2H), 3.58 (t, *J* = 6 Hz, 2H), 3.22 (t, *J* = 5.6 Hz, 4H), 1.33 (d, , *J* = 17.6 Hz, 20H); **^{13}C NMR (100 MHz, DMSO-*d*$_6$/CDCl$_3$(1:1)):** *δ* 164.8, 131.5, 108.8, 73.6, 66.3, 41.4, 36.0, 34.5, 24.6, 23.5, 23.3; **HRMS (ESI):** Calc. for $C_{22}H_{35}N_2O_6$ [M+H]$^+$: 423.2488; Found: 423.2495.

III. Ion Transport Studies by Fluorescence

Buffer and stock solution preparation: HEPES buffer (10 mM) was prepared by dissolving solid HEPES in autoclaved water, then NaCl (100 mM) was added and followed by adjustment of pH = 7.0 by adding NaOH solution. Stock solutions of all compounds were prepared in either HPLC grade DMSO (for HPTS assay) and in 1:1 MeOH/THF (for Lucigenin assay).

Preparation of EYPC-LUVs⊃HPTS: Vesicles were prepared according to reported protocol.[S9-11]
Ion transport activity: 1975 μL of HEPES buffer (10 mM HEPES, 100 mM NaCl, pH = 7.0) was taken in a clean fluorescence cuvette followed by addition of 25 μL of EYPC-LUVs⊃HPTS in the same cuvette and was placed on the fluorescence instrument (at *t* = 0 s) equipped with magnetic stirrer. Fluorescence emission intensity of HPTS dye, F_t was monitored at λ_{em} = 510 nm (λ_{ex} = 450 nm) with time. After that a pH gradient between the intra and extra vesicular system was created by adding 20 μL of 0.5 M NaOH to the same cuvette at *t* = 20 s (Fig. S1). All compounds were added at *t* = 100 s in different concentrations and finally at *t* = 300 s, 25 μL of 10% Triton X-100 was added to destroy all vesicles which resulted in destruction of pH gradient (Fig. S1) which resulted in saturation in fluorescence emission intensity.

The time axis was normalized according to Equation S1:

$$t = t - 100 \quad \text{(S1)}$$

The time of compound addition can be normalized to t = 0 s and time of Triton-X 100 addition was normalized to t = 200 s.

Fluorescence intensities (F_t) were normalized to fractional emission intensity I_F using Equation S2:

$$I_F = [(F_t - F_0)/(F_\infty - F_0)] \times 100 \quad \text{(S2)}$$

Where F_0 = Fluorescence intensity just before the compound addition (at t = 0 s). F_∞ = Fluorescence intensity at saturation after complete leakage (at t = 330 s). F_t = Fluorescence intensity at time t.

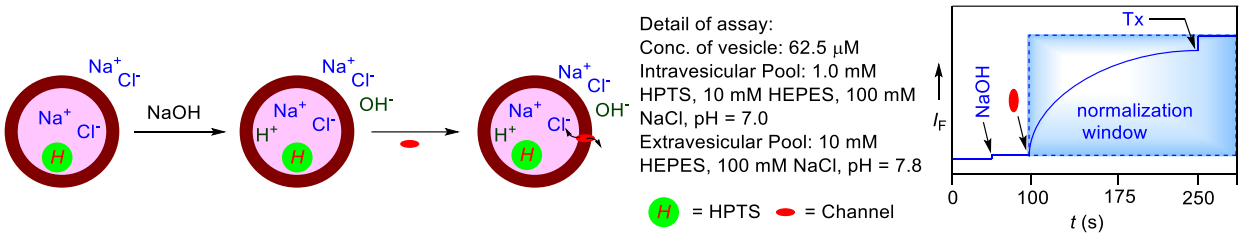

Fig. S1 Representation of ion transport activity assay using EYPC-LUVs⊃HPTS.

Ion transport kinetics were studied at different concentrations for each compound. Change of HPTS emission intensity in this process was monitored with time.

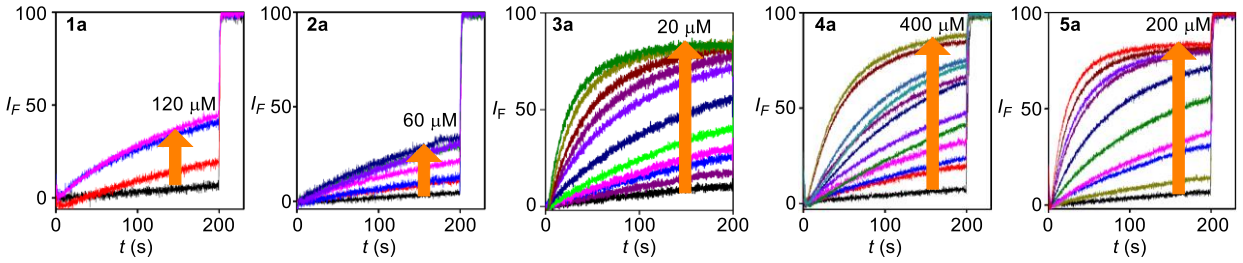

Fig. S2 Concentration dependent ion transport activity of fumaramides **1a** – **5a** across EYPC-LUVs⊃HPTS.

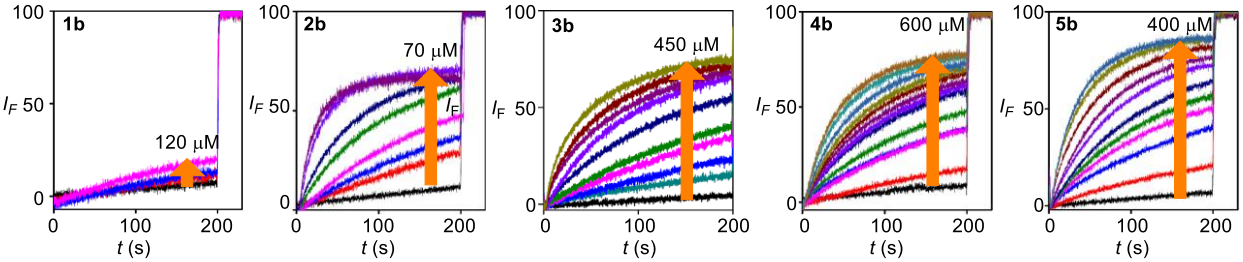

Fig. S3 Concentration dependent ion transport activity of maleamides **1b** – **5b** across EYPC-LUVs⊃HPTS.

The concentration profile data were analyzed by Hill Equation (Equation S3) to get the Effective concentration at half maximal activity (EC_{50}) and Hill Coefficient *(n)*,

$$Y = Y_\infty + (Y_0 - Y_\infty) / [1 + (c / EC_{50})^n] \quad \text{(S3)}$$

Where, Y_0 = Fluorescence intensity just before the channel forming molecule addition (at 0 s). Y_∞ = Fluorescence intensity with excess channel concentration, c = Concentration of channel forming molecule.

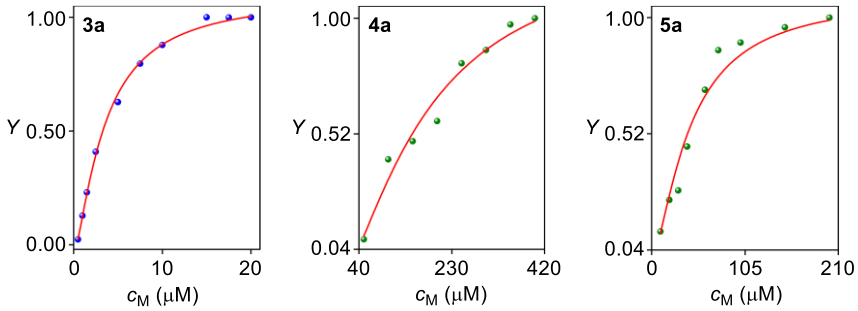

Fig. S4 Hill plots of **3a** – **5a** obtained from concentration dependent HPTS assay.

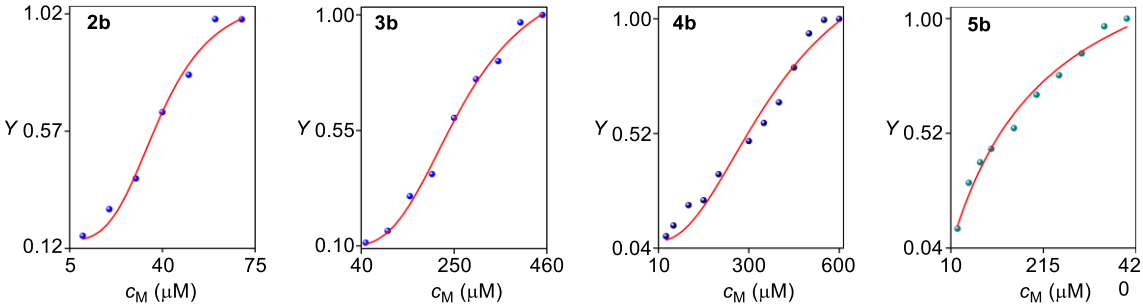

Fig. S5. Hill plots of **2b** – **5b** obtained from concentration dependent HPTS assay.

Ion transport activity in the presence of FCCP:[S7] In a clean and dry fluorescence cuvette 1975 μL of HEPES buffer (10 mM HEPES, 100 mM NaCl, pH = 7.0) was taken followed by addition of 25 μL of EYPC-LUVs⊃HPTS in stirring condition by a magnetic stirrer equipped with the fluorescence instrument (at t = 0 s). HPTS fluorescence emission intensity was monitored with time and F_t was observed at λ_{em} = 510 nm (λ_{ex} = 450 nm). At t = 20 s, 20 μL of 0.5 M NaOH was added to the cuvette to make the pH gradient between the intra and extra vesicular solution. FCCP (2.5 μM) was added at t = 50 s (whenever necessary) and channel molecule was added at t = 100 s (whenever necessary) and finally at t = 300 s 25 μL of 10% Triton X-100 was added to that cuvette resulting destruction of pH gradient. Fluorescence intensities (F_t) were normalized to fractional emission intensity I_F using Equation S2 and time scale was normalized according to Equation S1.

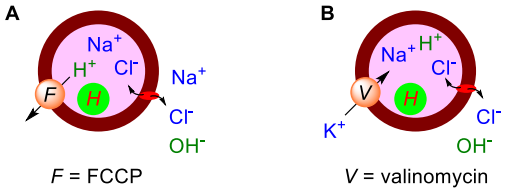

Fig. S6 Representations of fluorescence based FCCP (**A**) and Valinomycin (**B**) assays across EYPC-LUVs⊃HPTS.

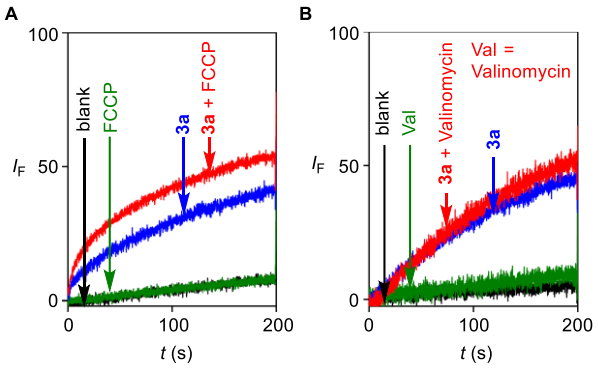

Fig. S7. Ion transport activity of compound **3a** (3.5 μM) determined in the absence and in the presence of FCCP (**A**); and ion transport activity of compound **3a** (3.5 μM) determined in the absence and in the presence of valinomycin (**B**).

Ion transport activity in the presence of valinomycin:[S7] In a clean and dry fluorescence cuvette 1975 μL of HEPES buffer (10 mM HEPES, 100 mM NaCl, pH = 7.0) was added followed by addition of 25 μL of EYPC-LUVs⊃HPTS in slowly stirring condition by a magnetic stirrer equipped with the fluorescence instrument (at t = 0 s). The time course of HPTS fluorescence emission intensity, F_t was observed at λ_{em} = 510 nm (λ_{ex} = 450 nm). 20 μL of 0.5 M NaOH was added to the cuvette at t = 20 s to make the pH gradient between the intra and extra vesicular system. Valinomycin (2.5 pM) was added at t = 50 s (whenever necessary) and channel molecule was added at t = 100 s (whenever necessary) and finally at t = 300 s 25 μL of 10% Triton X-100 was added to lyse those vesicles resulting destruction of pH gradient. Fluorescence intensities (F_t) were normalized to fractional emission intensity I_F using Equation S2.

Ion Selectivity Assay:

Buffer and stock solution preparation: HEPES buffer was prepared by dissolving solid HEPES (10 mM) and appropriate salts (100 mM) in autoclaved water, followed by adjustment of pH = 7.0 by adding NaOH solution. Stock solutions of all channel forming molecules were prepared in DMSO (for HPTS assay) of HPLC grade.

Preparation of EYPC-LUVs⊃HPTS: Vesicles were prepared according to the procedure discussed earlier.

Ion Selectivity Assay: In a dry and clean fluorescence cuvette HEPES buffer (10 mM HEPES, 100 mM NaCl, pH = 7.0) 1975 μL was added followed by addition of 25 μL of EYPC-LUVs⊃HPTS in stirring condition by a magnetic stirrer equipped with the fluorescence instrument (at t = 0 s). Fluorescence intensity, F_t of HPTS dye was measured at λ_{em}= 510 nm (λ_{ex}= 450 nm) with time. pH gradient between the intra and extra vesicular system was created by applying 20 μL of 0.5 M NaOH to the cuvette at t = 20 s. All molecules were added at t = 100 s and at t = 300 s, of 10% Triton X-100 (25 μL) was added to lyse all the vesicles for complete destruction of pH gradient. All fluorescence kinetics data were normalized between 0 (at t = 96 s) and 100 (at t = 330 second) by using equation S2 and time was normalized by Equation S1.

Cation selectivity assay was carried out by varying the extravesicular chloride salts (MCl) of different alkali metal cations. Insignificant difference in rate was observed for different cations (M^+ = Li^+, Na^+, K^+, Rb^+, and Cs^+) indicating that compound was not selective towards cation.

Anion selectivity compound **3a** were evaluated by varying the extravesicular sodium salts of different anions (X^- = Cl^-, Br^-, I^-, NO_3^-, SCN^-, and ClO_4^-). The difference in rate observed for different anions is characteristics of anion selectivity. Difference in transport activity was observed due to the competitive transport of X^-/OH^-.

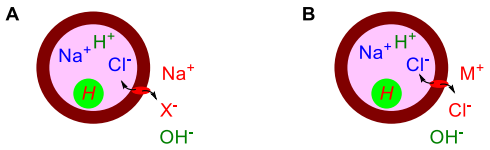

Fig. S8 Schematic representations of the HPTS fluorescence based selectivity assay for anion (**A**) and cation (**B**).

Determination of chloride ion selectivity by lucigenin assay:[S6]

Preparation of EYPC-LUVs⊃Lucigenin vesicles: 1 mL solution of EYPC (25 mg) lipid dissolved in $CHCl_3$ was taken in a clean and dry small round bottom flask. The solvents were evaporated slowly by a stream of nitrogen, followed by drying under vacuum for 4-5 h. After that 1 mL of 1 mM lucigenin (*N,N′*-Dimethyl-9,9′-biacridinium dinitrate) in 200 mM $NaNO_3$ (dissolved in water) was added to the round bottom flask, and the suspension was hydrated for 1 h with occasional vortexing of 4-5 times and then subjected to freeze-thaw cycle (≥ 15 times). The vesicle solution was extruded through a polycarbonate membrane with 200 nm pores for minimum 19 times (must be an odd number), to give vesicles with a mean diameter of ~ 200 nm. The extracellular lucigenin was removed from the vesicles by size exclusion column chromatography (Sephadex G-50) using 200 mM $NaNO_3$ as eluent. The obtained vesicles were diluted to 4 mL with 200 mM $NaNO_3$.

Determination of chloride ion selectivity by lucigenin assay: In a clean and dry fluorescence cuvette 50 µL of above lipid solution and 1950 µL of 200 mM $NaNO_3$ solution was taken and kept in slowly stirring condition by a magnetic stirrer equipped with the fluorescence instrument (at t = 0 s). In this assay, the time course of lucigenin fluorescence emission intensity, F_t was observed at λ_{em} = 535 nm (λ_{ex} = 455 nm). 25 µL of 2 N NaCl was added to the cuvette at t = 50 s to make the salt gradient between the intra and extra vesicular system. Ion channel forming molecule was added at t = 100 s and finally at t = 300 s, 25 µL of 10% Triton X-100 was added to lyse all vesicles for 100% chloride influx. Fluorescence intensities (F_t) were normalized to fractional emission intensity I_F using Equation S4.

$$I_F = [(F_t - F_0) / (F_\infty - F_0)]\times(-1) \qquad \text{(S4)}$$

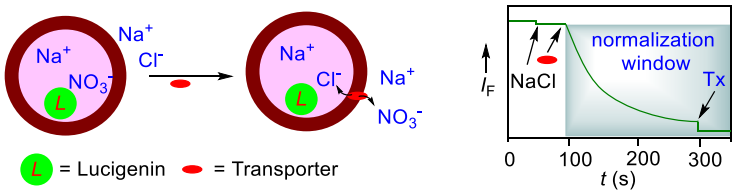

Fig. S9 Representation of chloride influx assay by monitoring the quenching of lucigenin fluorescence entrapped in EYPC-LUVs.

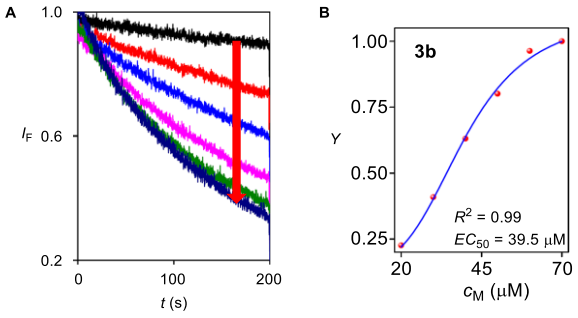

Fig. S10 Cl^- influx study with **3a** (0–60 µM) across EYPC-LUVs⊃Lucigenin vesicles (**A**). Representation of Hill plots for compound **3a** from Lucigenin assay (**B**).

To quantify transport abilities of compound **3a**, half-lives ($t_{1/2}$) and initial rates (I_R) were calculated. Half-lives ($t_{1/2}$) of transport activities were obtained by fitting fluorescence quenching curve of compound **3a** (at 40 μM) to a single exponential decay function with Equation S5 and followed by calculation of half-life by Equation S6.

$$I/I_0 = a + b.e^{-ct} \quad \text{(S5)}$$

$$t_{1/2} = 0.693/c \quad \text{(S6)}$$

Initial rate, I_R for the transport process was obtained by fitting fluorescence quenching curve with the double exponential decay equation,

$$I/I_0 = y_0 + a.^{(-bt)} + c.e^{(-dt)} \quad \text{(S7)}$$

Now, differentiating with respect to *t* gives:

$$\partial y/\partial t = a.b.^{(-bt)} + \text{c}.d.e^{(-bt)} \quad \text{(S8)}$$

Initial rate I_R was calculated by putting $t = 0$ s in the above equation:

$$I_R = \partial y/\partial t_{t=0} = a.b + c.d \quad \text{(S9)}$$

Initial rates I_R at other concentrations were also calculated.

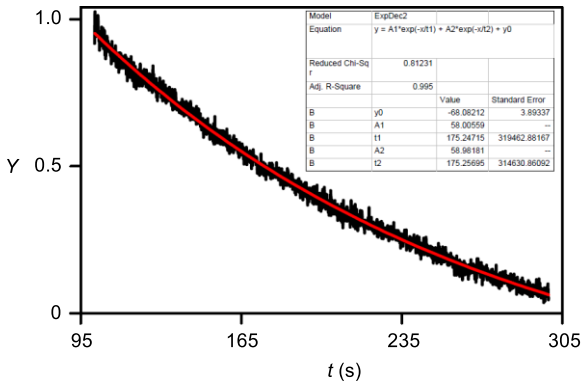

Fig. S11 Representation of fitting plot of compound **3a** (40 μM) to calculate initial rate (I_R) and half-life ($t_{1/2}$).

Chloride influx activity in the presence of valinomycin:[S6] In a clean and dry fluorescence cuvette 50 μL of lipid solution and 1950 μL of 200 mM $NaNO_3$ solution was taken and kept in slowly stirring condition by a magnetic stirrer equipped with the fluorescence instrument (at $t = 0$ s). In this assay, the time course of lucigenin fluorescence emission intensity, F_t was observed at λ_{em} = 535 nm (λ_{ex} = 450 nm). 25 μL of 2 N KCl was added at $t = 20$ s, valinomycin was added at $t = 50$ s followed by compound **3a** at $t = 100$ s and finally at $t = 300$ s, 25 μL of 10% Triton X-100 was added to lyse all vesicles for 100% chloride influx. Fluorescence intensities (F_t) were normalized to fractional emission intensity I_F using Equation S4.

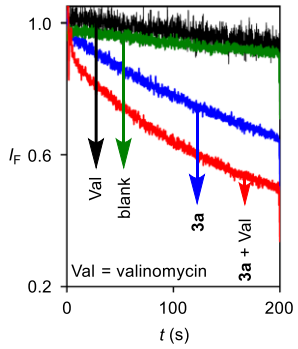

Fig. S12 Cl^- influx study with **3a** (30 µM) in the absence and presence of valinomycin.

Preparation of EYPC-LUVs⊃CF:[S6] A thin lipid film was prepared by evaporating a solution of 12.5 mg EYPC in 0.5 ml $CHCl_3$ in vacuo for 4 h. After that lipid film was hydrated with 0.5 mL buffer (10 mM HEPES, 10 mM NaCl, 50 mM CF, pH 7.0) for 1 h with occasional vortexing of 4-5 times and then subjected to freeze-thaw cycle (≥ 20 times). The vesicle solution was extruded through a polycarbonate membrane with 100 nm pores 19 times (has to be an odd number), to give vesicles with a mean diameter of ~ 100 nm. The extracellular dye was removed size exclusion chromatography (Sephadex G-50) with 10 mM HEPES buffer (100 mM NaCl, pH 7.0. Final) Final concentration: ~2.5 mM EYPC lipid; intravesicular solution: 10 mM HEPES, 10 mM NaCl, 50 mM CF, pH 7.0; extravesicular solution: 10 mM HEPES, 100 mM NaCl, pH 7.0.

CF leakage assay: In a clean and dry fluorescence cuvette 25 µL of above lipid solution and 1975 µL of 10 mM HEPES buffer (100 mM NaCl, pH 7.0) was taken and kept in slowly stirring condition by a magnetic stirrer equipped with the fluorescence instrument (at t = 0 s). The time course of CF fluorescence emission intensity, F_t was observed at λ_{em} = 517 nm (λ_{ex} = 492 nm). Compound **3a** was added at t = 100 s and finally at t = 300 s, 25 µL of 10% Triton X-100 was added to lyse those vesicles for 100% chloride influx. Fluorescence intensities (F_t) were normalized to fractional emission intensity I_F according to Equation S2. This study confirmed that neither the bilayer membranes are defected nor large transmembrane pores are formed by **3a**.

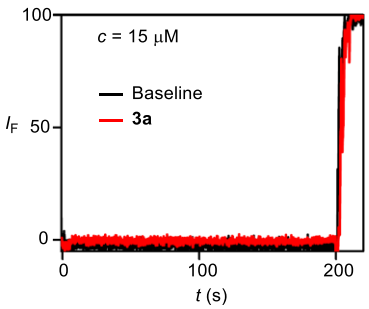

Fig. S13 Carboxyfluorescein efflux assay for compound **3a** (15 µM).

IV. Planar Bilayer Conductance Measurements

Bilayer membrane (BLM) was formed across an aperture of 150 µM diameter in a polystyrene cup (Warner Instrument, USA) with lipid diphytanoylphosphatidylcholine (Avanti Polar Lipids), dissolved in *n*-decane (18 mg/mL). Both chambers (*cis* and *trans*) were filled with symmetrical solution, containing 1 M KCl. The *trans* compartment was held at virtual ground and the *cis* chamber was connected to the BC 535 head-stage (Warner Instrument, USA) via matched Ag-AgCl electrodes. Compound **3a** (20 µM) was added to the *trans* chamber and the solution was stirred with magnetic stirrer for 10 min. Channel formation was confirmed by the distinctive channel opening and closing events after applying voltages.

Currents were low pass filtered at 1 kHz using pClamp9 software (Molecular probes, USA) and analog-to-digital converter (Digidata 1440, Molecular probes). All data were analyzed by the software pClamp 9.

The complete data trace observed for ten minutes contained a series of opening and closing events at some indefinite intervals. On an average 7-8 transitions per minute were observed. From this complete trace a small portion is presented in the manuscript (Fig. 4A, B). The average current was calculated from this trace and then conductance and other calculations were made accordingly.

Calculation of ion channel diameter: Diameter of artificial ion channel was calculated according to Hille's equation,

$$1/g = (l + \pi d/4) \times (4\rho / \pi d^2) \quad \text{(S10)}$$

Where, g = corrected conductance (obtained by multiplying measured conductance with the Sansom's correction factor) = 3.37×10^{-10} S, l = length of the ion channel = 37 Å, and ρ = resistivity of the 1 M KCl solution = 9.47 Ω·cm).

Determination of permeability ratio: The *cis* and *trans* chambers were filled with unsymmetric solutions of KCl. The *cis* chamber was filled with 1.0 M KCl solution and *trans* chamber was filled with 0.5 M KCl. The compound **3a** (20 μM) was added to the *trans* chamber and stirred for 20 minutes. The reversal potential was calculated to be 16 ± 2 mV (Fig. 4C).

The permeability ratio (P_{Cl-}/P_{K+}) was calculated by using Goldman-Hodgkin-Katz equation[S12] (Equation S11).

$$\frac{P_{Cl^-}}{P_{K^+}} = \frac{a_{K^+_{cis}} - a_{K^+_{trans}} \times \exp\left(-\frac{V_{rev} \times F}{R \times T}\right)}{a_{Cl^-_{cis}} \times \exp\left(-\frac{V_r \times F}{R \times T}\right) - a_{Cl^-_{trans}}} \quad \text{(S11)}$$

where P_{Cl^-}/P_{K^+} = anion/cation permeability ratio; a_{K^+cis} = K^+ activity in the *cis* chamber; a_{K^+trans} = K^+ activity in the *trans* chamber; a_{Cl^-cis} = Cl^- activity in the *cis* chamber; a_{Cl^-trans} = Cl^- activity in the *trans* chamber; V_{rev} = reversal potential; F = Faraday constant; R = gas constant; T = temperature (K).

V. Crystal Structures[S13]

Crystal structures of two small-molecule fumaramides and two small-molecule maleamides were available at the Cambridge Structural Database (CSD). Hydrogen bonding interactions of these compounds were analyzed.

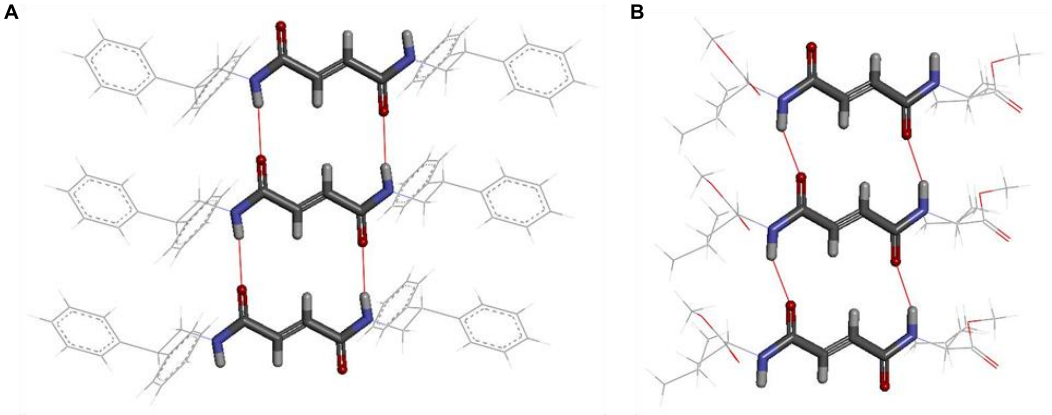

Fig. S14 Intermolecular hydrogen bonded packing pattern of reported small-molecule fumaramides. These crystal structures are taken from the references [S14] and [S15], respectively.

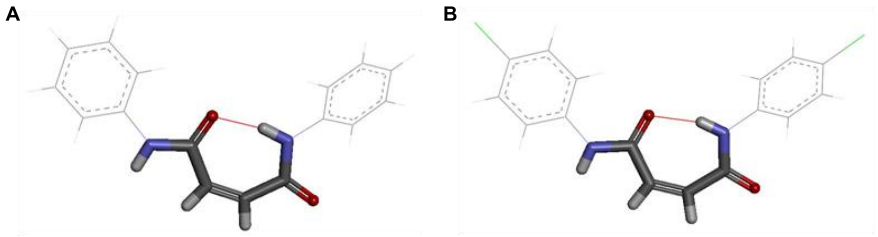

Fig. S15 Intramolecular hydrogen bonding interaction of reported small-molecule maleamides. These crystal structures are taken from the references [S16] and [S17], respectively.

Compounds **2a**, **3a** and **3b** were crystallized from chloroform/MeOH mixture at room temperature. Single-crystal X-ray data of compound **2a**, **3a** and **3b** were collected at 200 K on a Bruker KAPPA APEX II CCD Duo diffractometer (operated at 1500 W power: 50 kV, 30 mA) using graphite-monochromated Mo Kα radiation (λ = 0.71073 Å).[S18] The data integration and reduction were further processed with SAINT software. A multi-scan absorption correction was applied to the collected reflections. All those structures were solved by the direct method using SHELXTL and were refined on F^2 by full-matrix least-squares technique using the SHELXL-97 program package within the WINGX programme. All non-hydrogen atoms were refined anisotropically and all hydrogen atoms were located in successive difference Fourier maps and were treated as riding atoms using SHELXL default parameters. The structures were examined by using the *Adsym* subroutine of PLATON to confirm that no additional symmetry could be applied to the models. CCDC numbers for compound **2a**, **3a** and **3b** are 1534569, 1534571 and 1534570, respectively. These data can also be obtained free of charge from The Cambridge Crystallographic Data Centre.

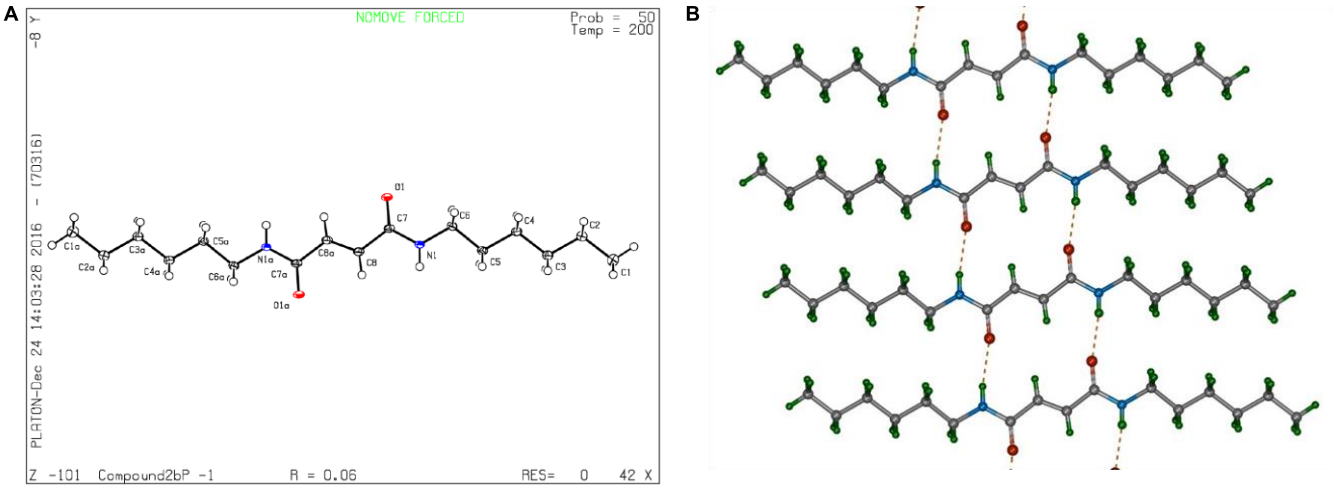

Fig. S16 ORTEP diagram of **2a** (**A**). Hydrogen bonded network of **2a** in the solid state (**B**).

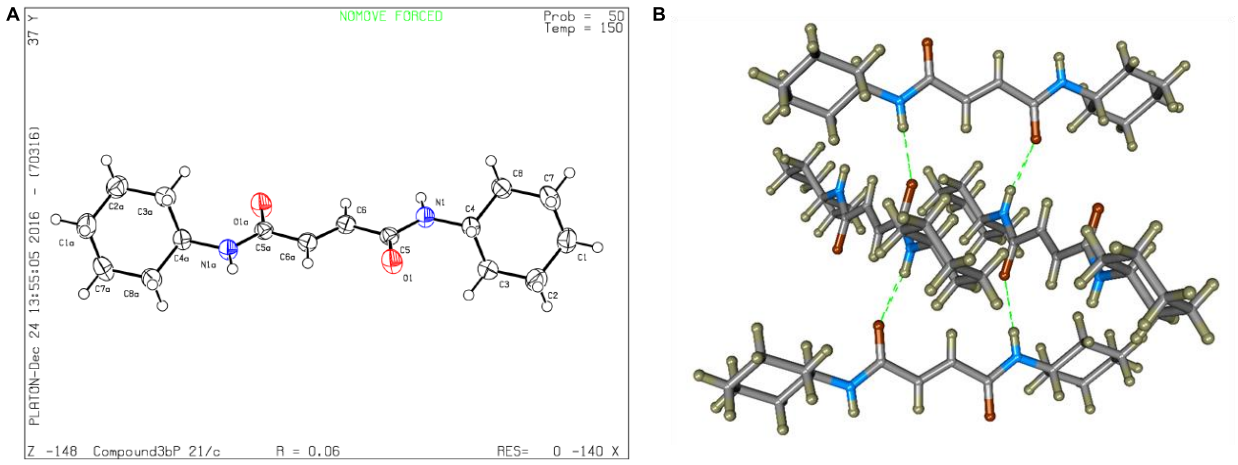

Fig. S17 ORTEP diagram of **3a** (**A**). Hydrogen bonded network of **3a** in ths solid state (**B**).

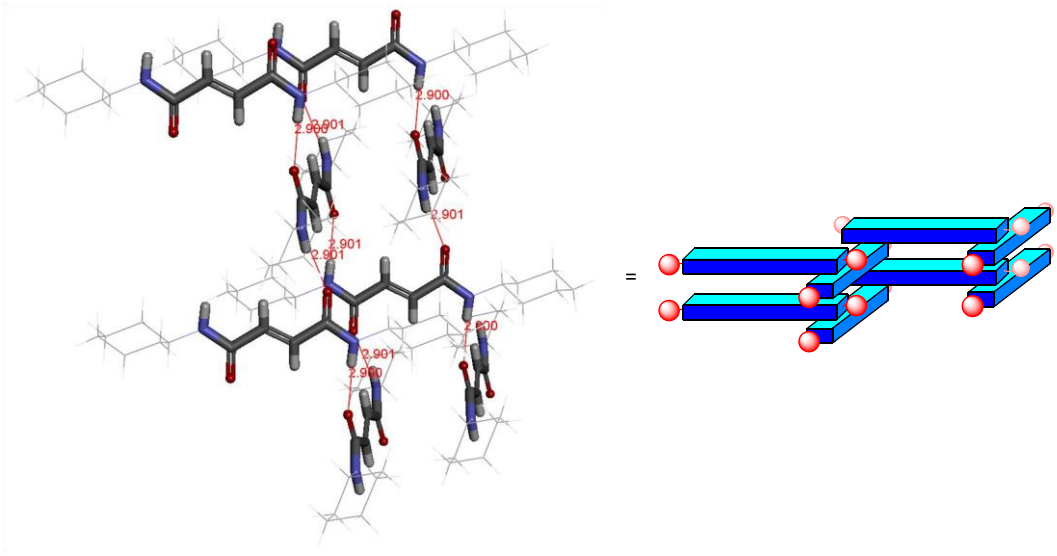

Fig. S18 Side-view of the hydrogen bonded *zig-zag* packing pattern in the crystal structure of **3a** and a cartoon representation of the same.

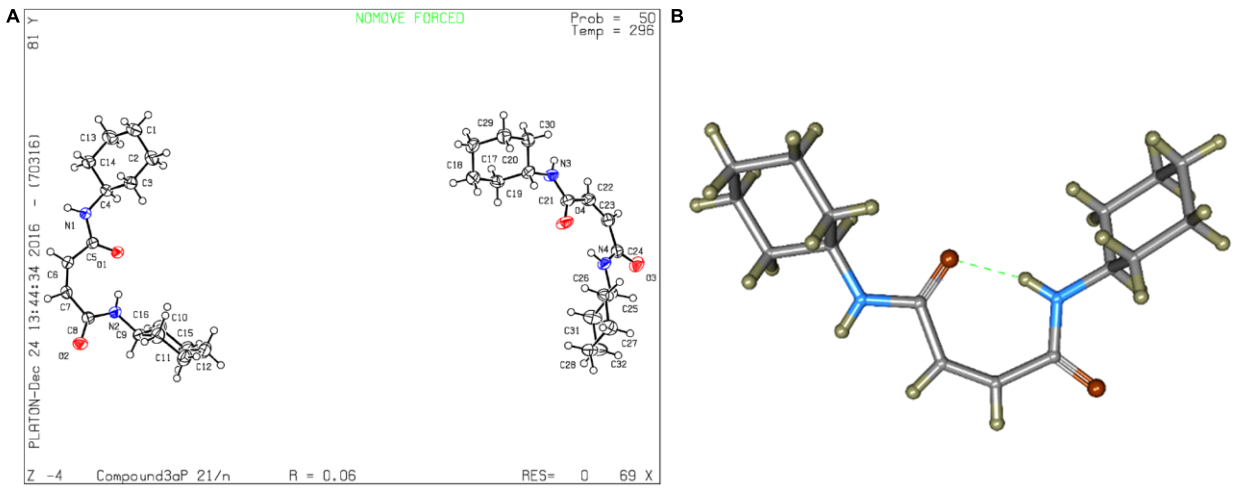

Fig. S19 ORTEM diagram of **3b** (**A**). Intramolecular hydrogen bonding interaction of **3b** (**B**).

VI. Molecular Modelling Studies

At first an all-atom model of the channel was built involving 16 molecules and the structure was optimized using MOPAC2012[S19] software with the PM6-DH+[S20] method (Fig. S19A-B). To investigate the chloride ion recognition, we placed the ion at either between the first and second layers or third and fourth layers of the model ion channel. Subsequently, these supramolecular complexes were also optimized. Fig. S20A-B represents the optimized structure with the chloride between the first and second layers. Fig. S21A-B represents the optimized structure with the chloride between the third and fourth second layers. The details about the optimizations are provided in the manuscript.

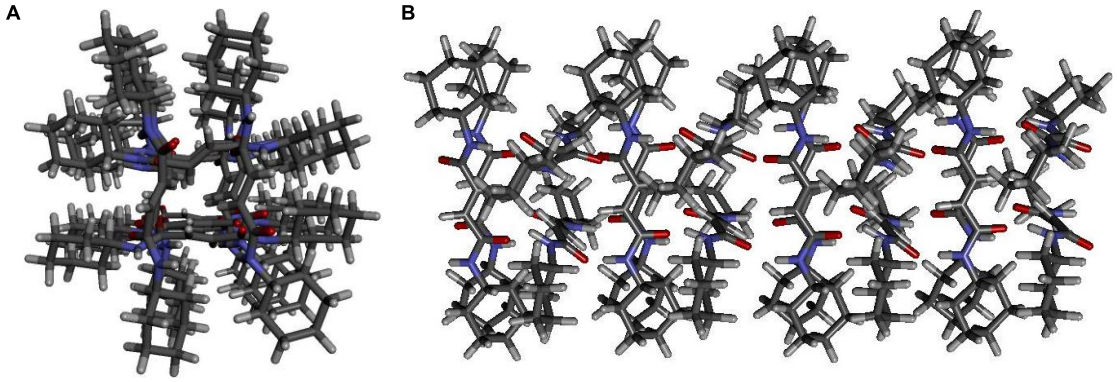

Fig. S20 Top view (**A**) and side view (**B**) of the optimized ion channel structure formed by **3a**.

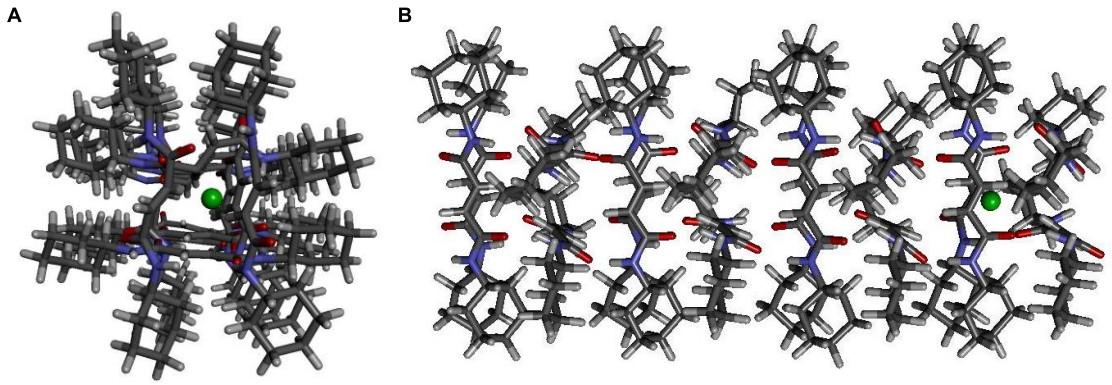

Fig. S21 Top view (**A**) and side view (**B**) of the optimized ion channel structure formed by **3a** in the presence of a Cl^- ion bound between the first and second layer of the channel.

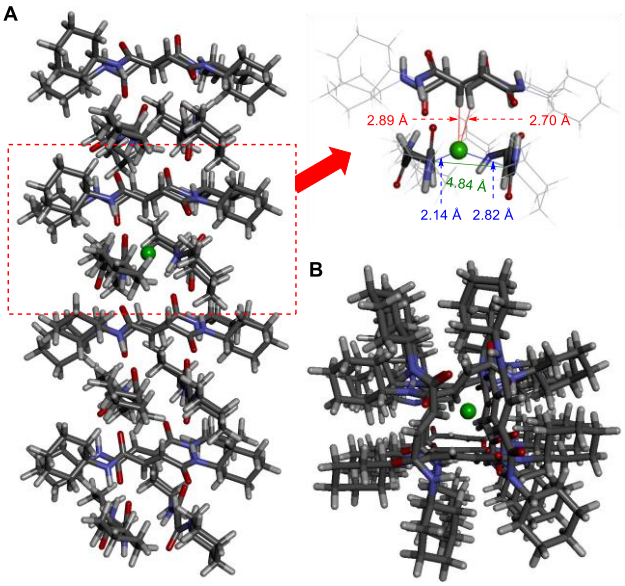

Fig. S22 Side view of geometry optimized structure of the channel with a Cl^- ion bound between the third and fourth layers of the channel (**A**). *Inset*: visualization of noncovalent interactions of the Cl^- ion with neighboring molecules. Top view of the same channel as **A** (**B**).

Subsequently, a chloride ion was placed between the third and fourth layers of the optimized channel, and two water molecules were placed near the ion (one above and the other below the ion). The generated structure was optimized further. The details about the optimizations are provided in the manuscript.

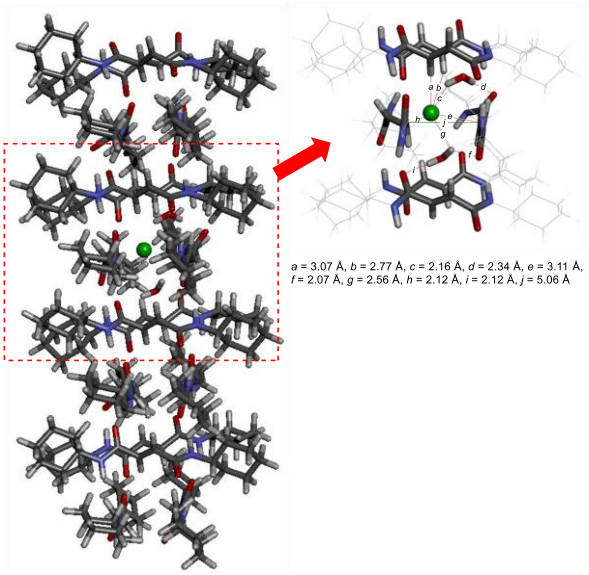

Fig. S23 Side view of geometry optimized structure of the channel with two water molecules and a Cl^- ion between the third and fourth layers of the channel. *Inset*: visualization of noncovalent interactions of the Cl^- ion with water and neighboring molecules.

VII. Photo-Responsive Ion Transport Studies

Photoisomerization of 3a: A solution of **3a** (1 mg/mL) in CH_3CN/CH_3OH (1:1) was irradiated for 30 min at room temperature using 290 nm (5 mW- 7 mW) pulse is generated from Optical Parametric Amplifier (TOPAS Prime). The optical parametric amplifier is fed by a regenerative amplifier (Spitfire, Spectra Physics) which generates pulses of 50 fs (FWHM), with 800 nm central wavelength at 1 kHz repetition rate. The completion of the reaction was monitored by thin layer TLC. The resulting sample was used directly for the ion transport studies by HPTS assay (as illustrated in Fig. S1).

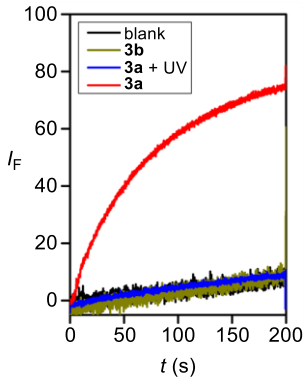

Fig. S24 Comparison of ion transport activities of **3a** (10 μM), **3b** (10 μM) and **3a** (10 μM) after photoisomerization.

VIII. NMR Spectra:

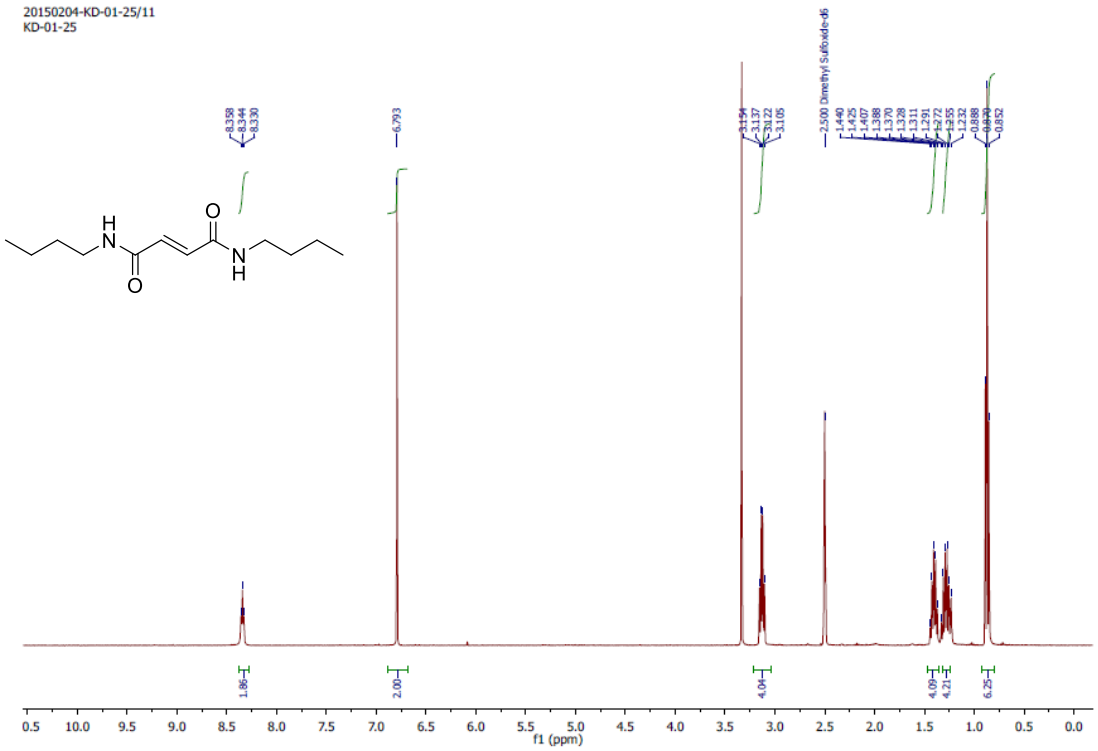

Fig. S25 ^{1}H NMR spectrum of **1a** in DMSO-d_6.

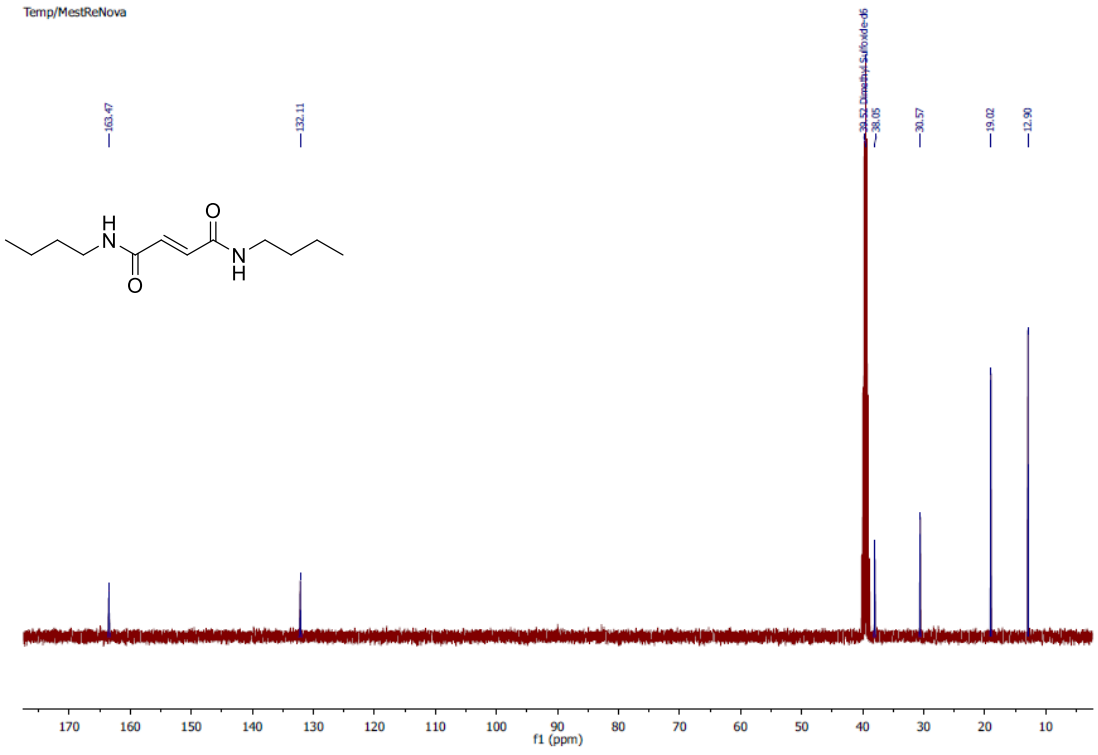

Fig. S26 ^{13}C NMR spectrum of **1a** in DMSO-d_6.

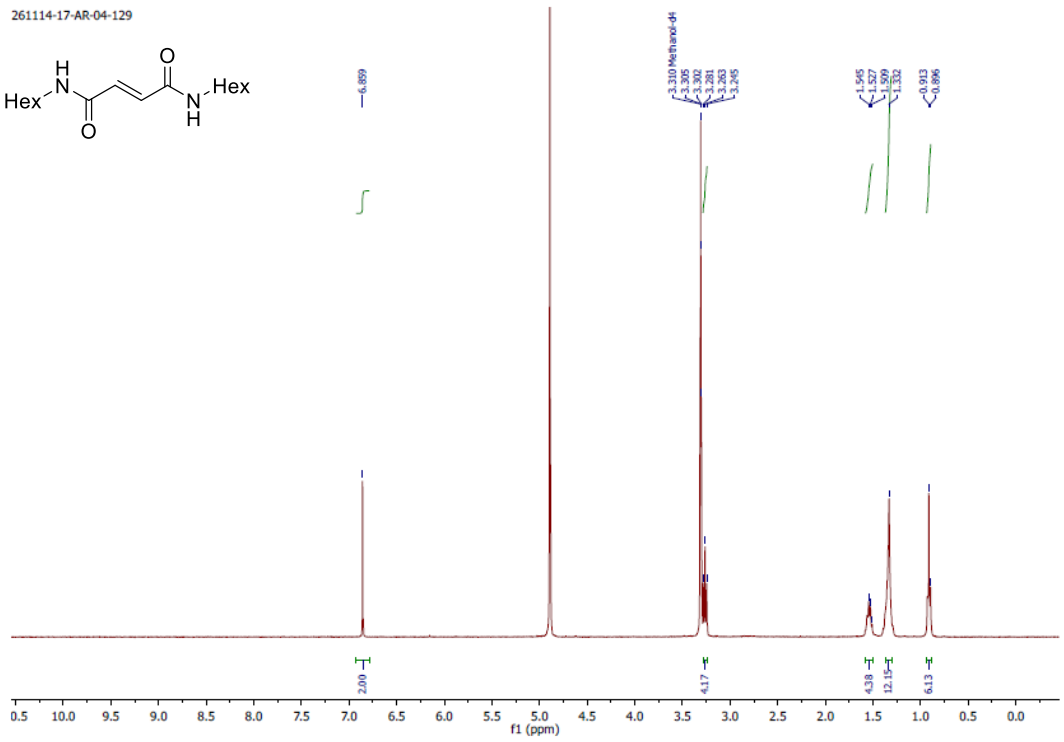

Fig. S27 ^{1}H NMR spectrum of **2a** in MeOH-d_4.

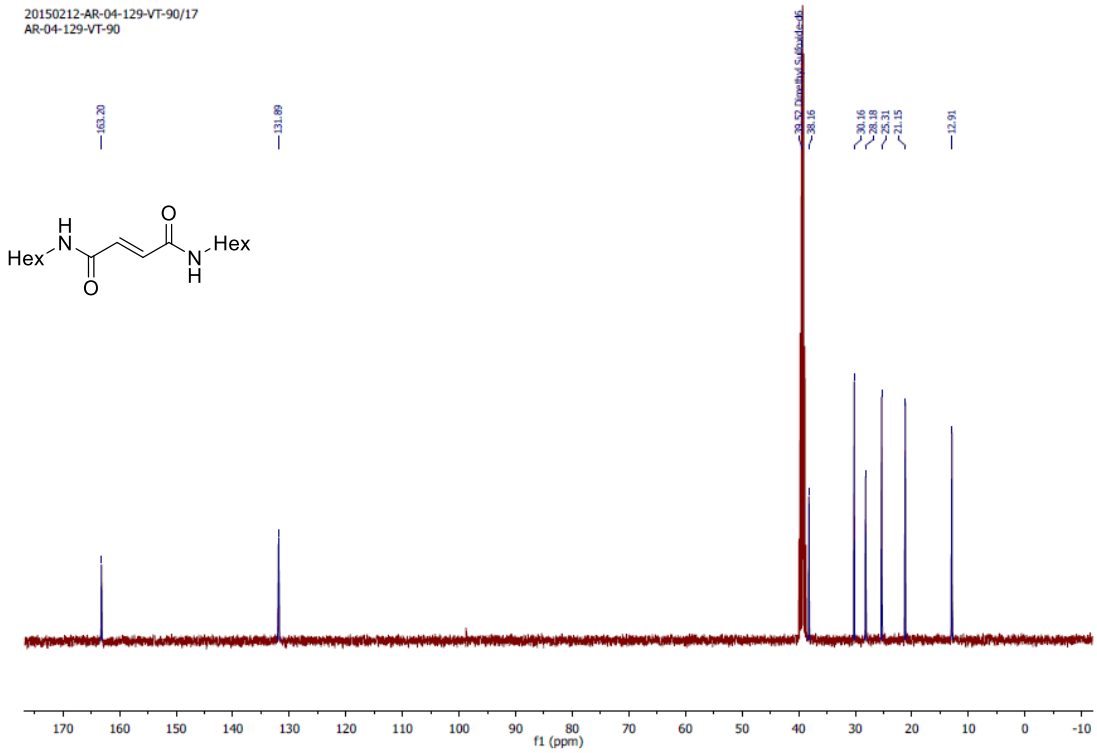

Fig. S28 ^{13}C NMR spectrum of **2a** in DMSO-d_6.

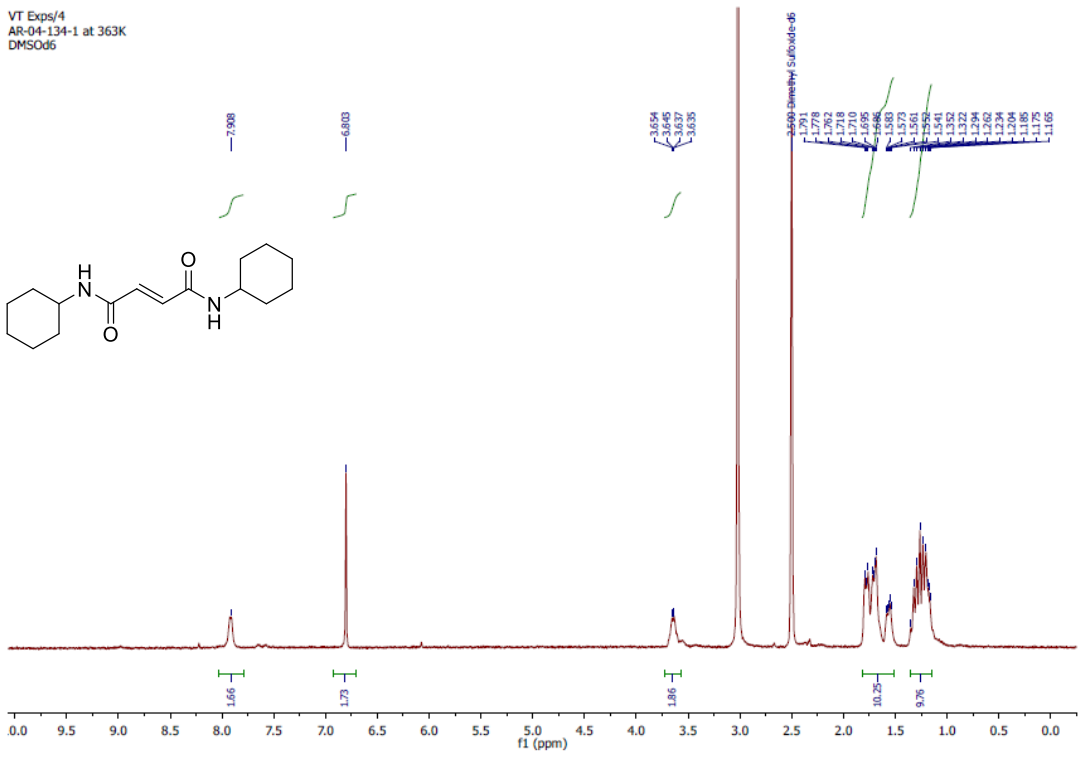

Fig. S29 ^{1}H NMR spectrum of **3a** in DMSO-d_6.

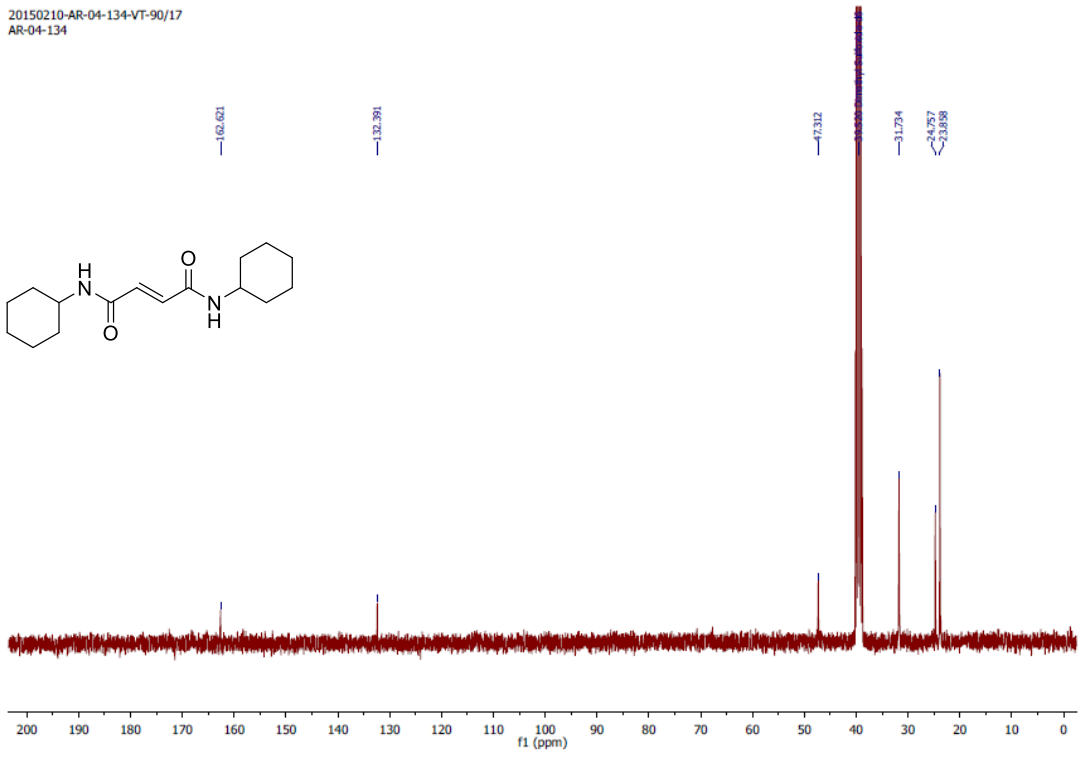

Fig. S30 ^{13}C NMR spectrum of **3a** in DMSO-d_6.

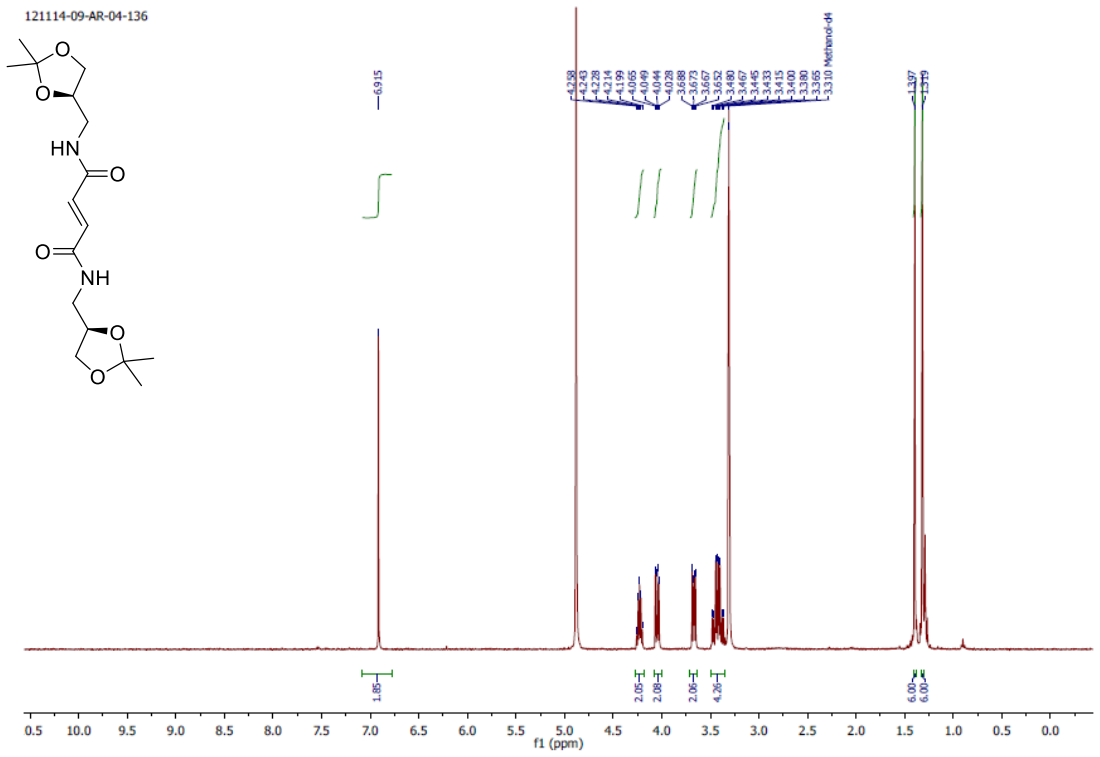

Fig. S31 ^{1}H NMR spectrum of **4a** in MeOH-d_4.

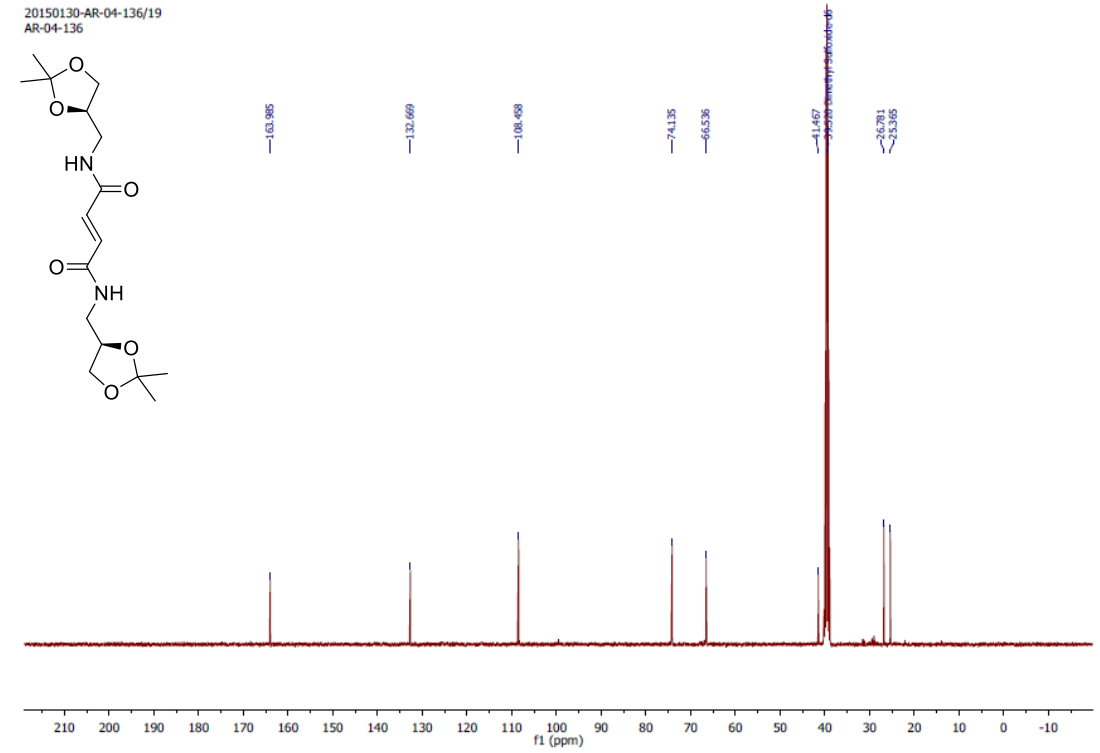

Fig. S32 ^{13}C NMR spectrum of **4a** in DMSO-d_6.

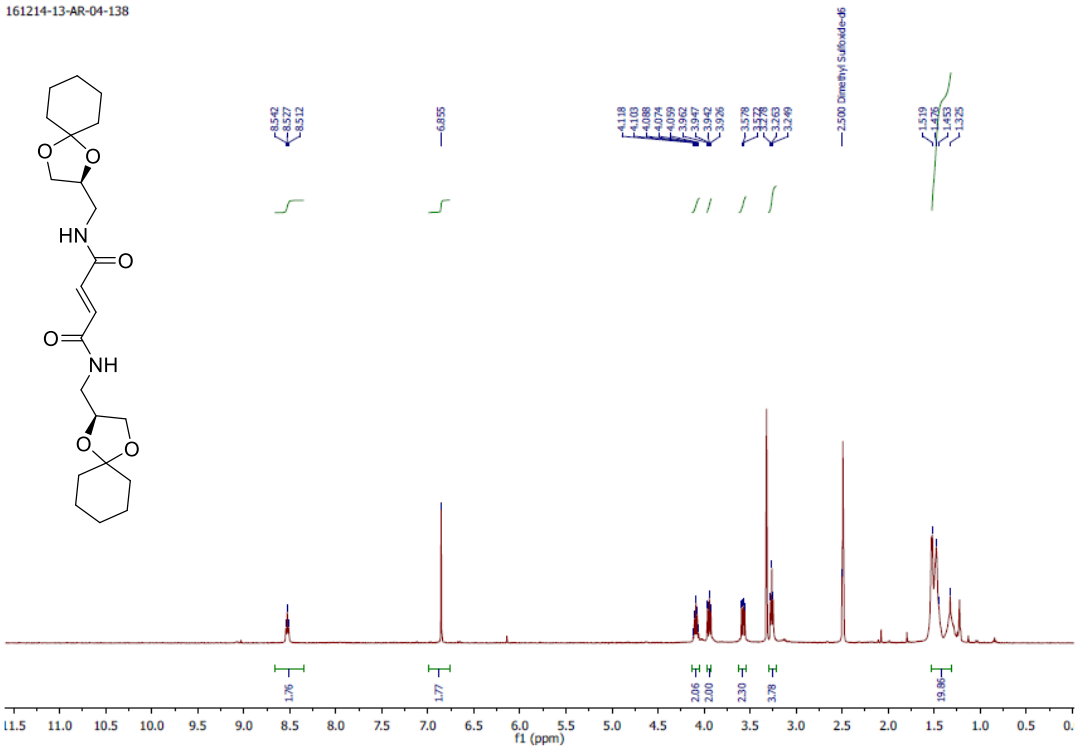

Fig. S33 ^{1}H NMR spectrum of **5a** in DMSO-d_6.

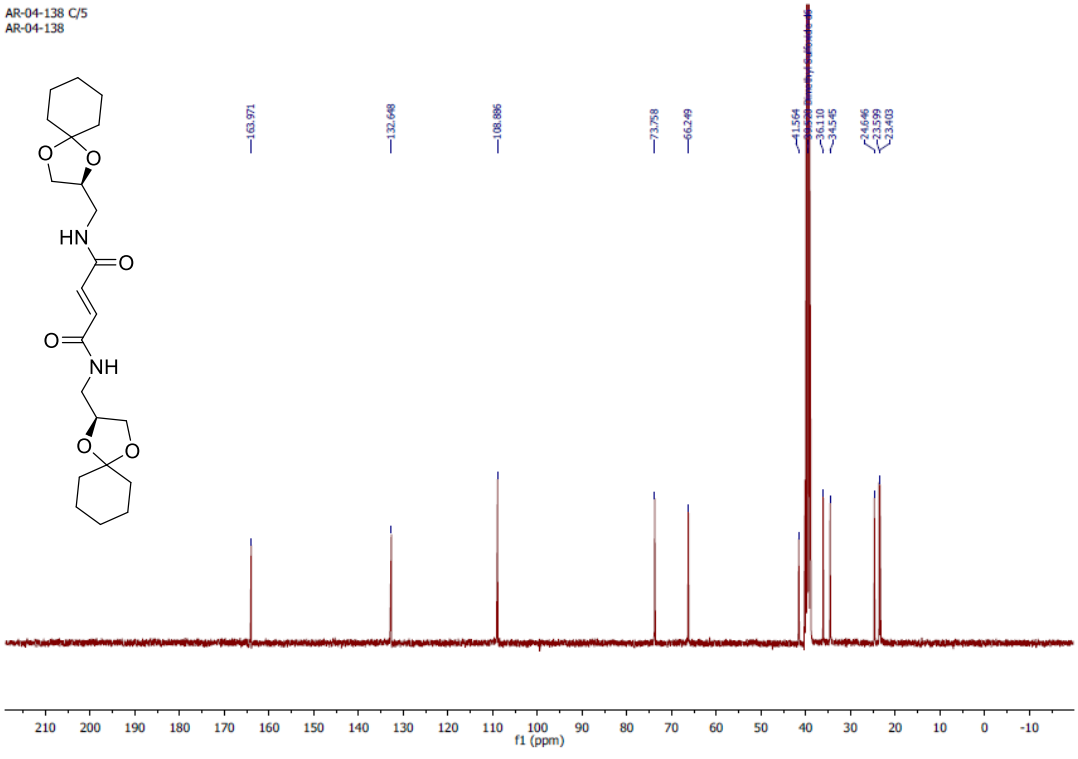

Fig. S34 ^{13}C NMR spectrum of **5a** in DMSO-d_6.

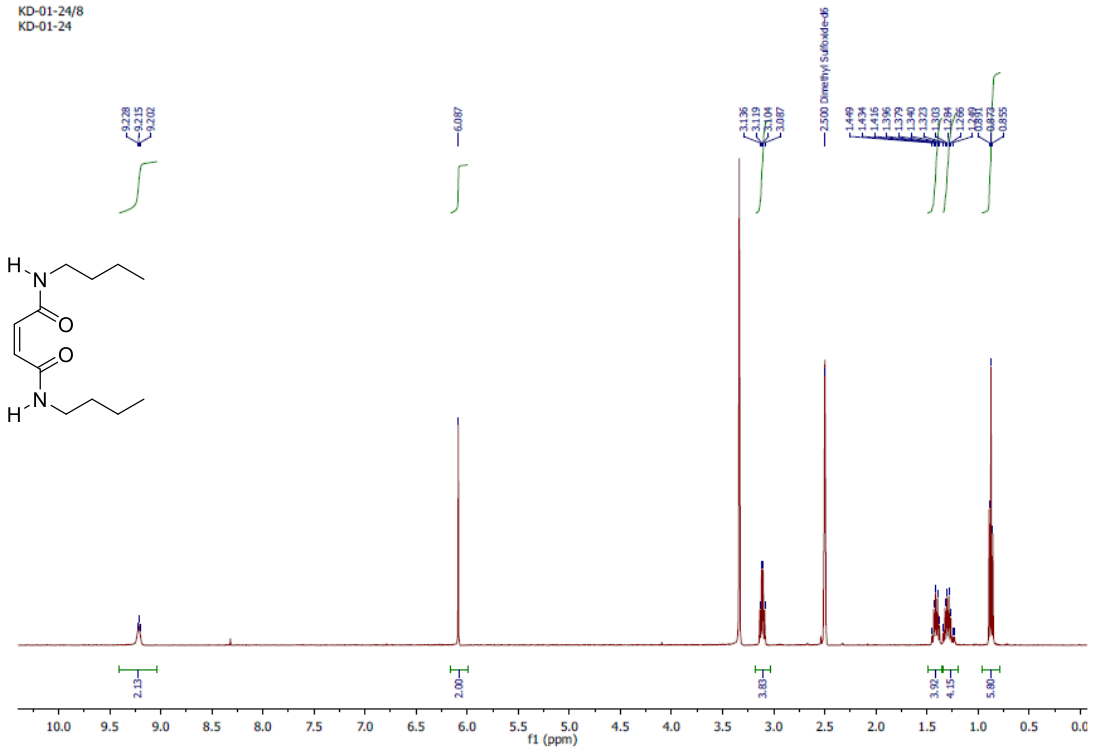

Fig. S35 ^{1}H NMR spectrum of **1b** in DMSO-d_6.

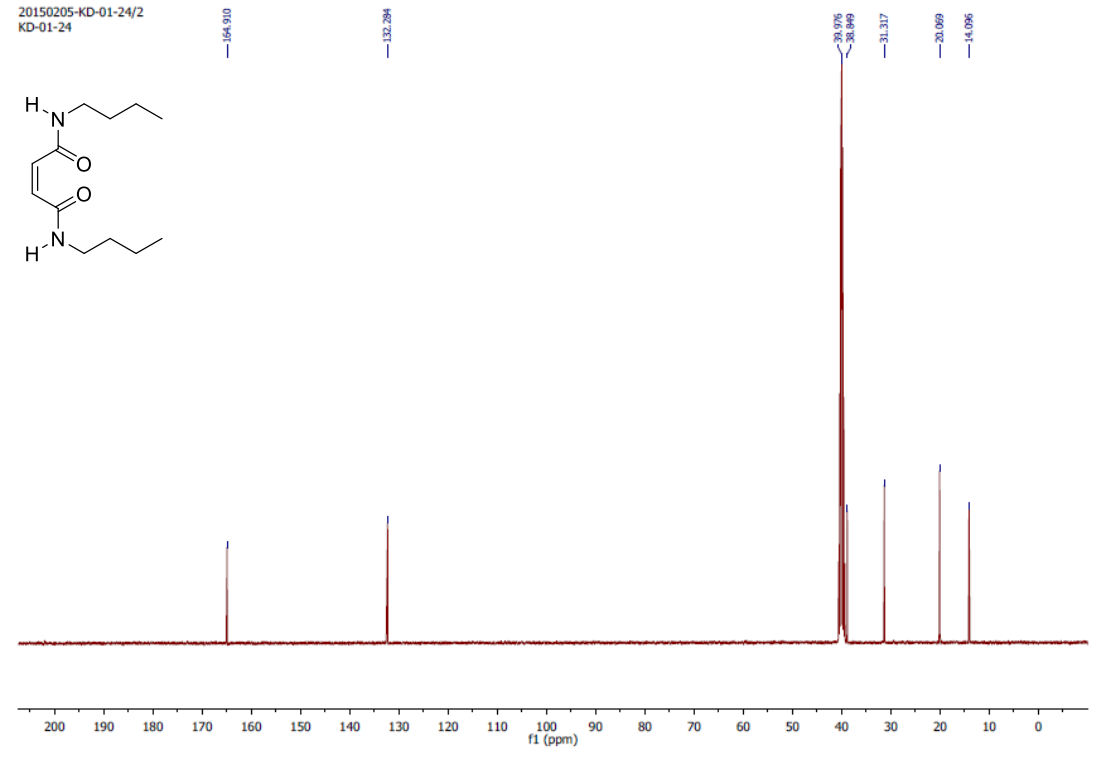

Fig. S36 ^{13}C NMR spectrum of **1b** in DMSO-d_6.

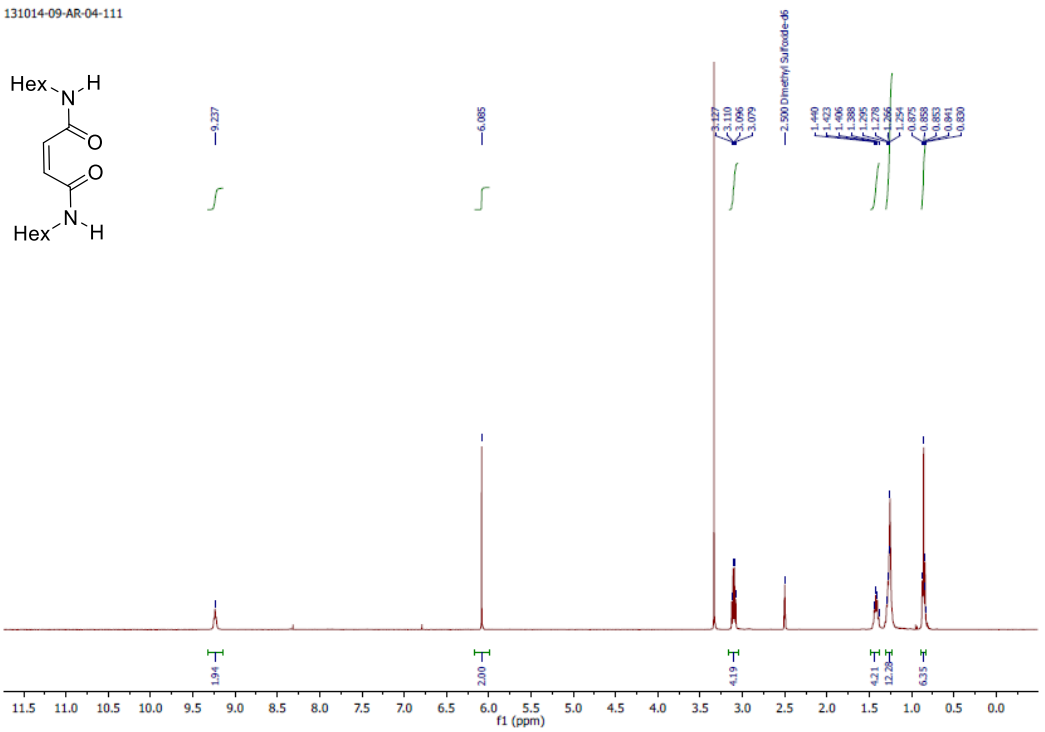

Fig. S37 ^{1}H NMR spectrum of **2b** in DMSO-d_6.

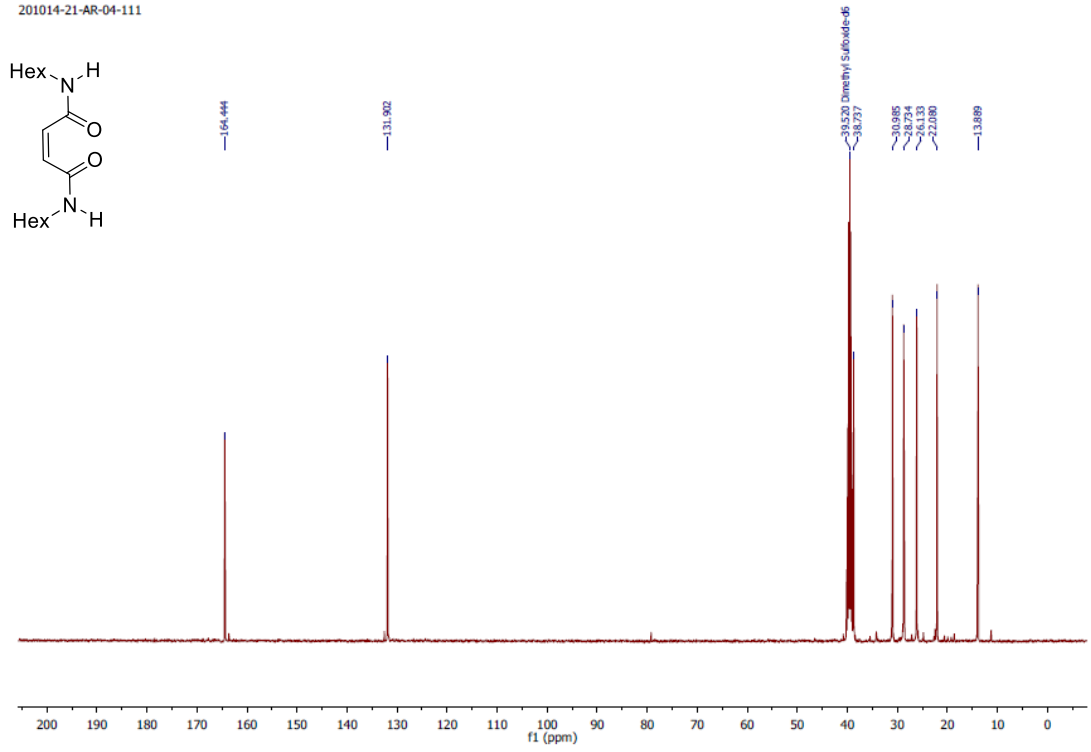

Fig. S38 ^{13}C NMR data of **2b** in DMSO-d_6.

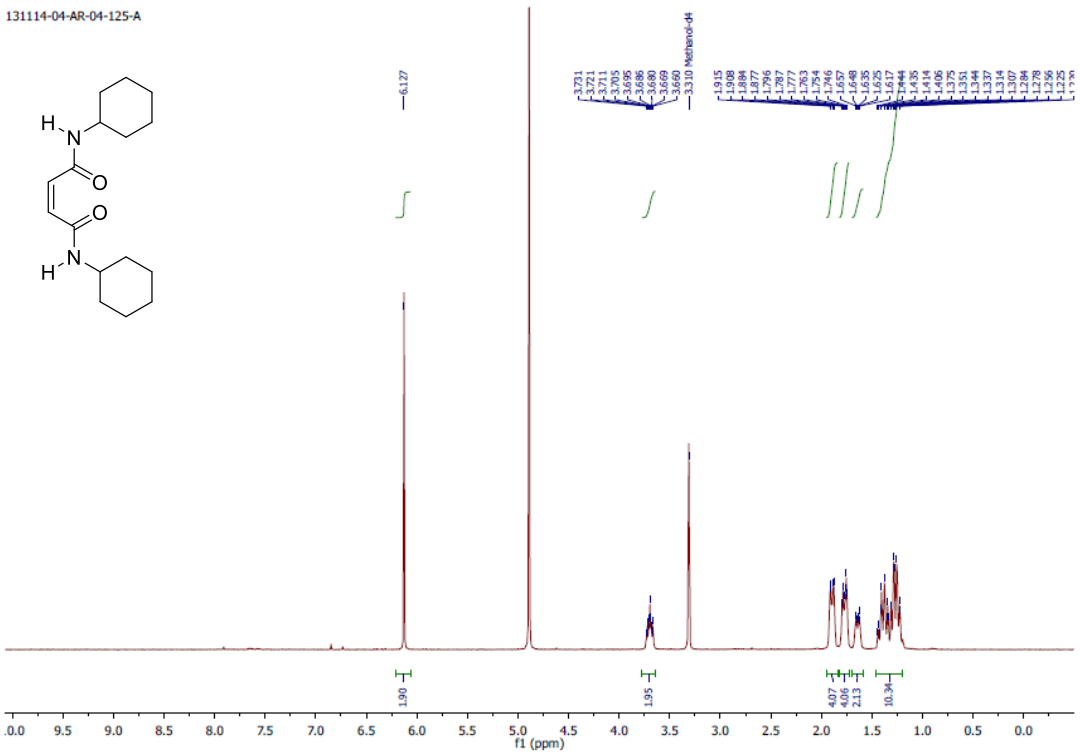

Fig. S39 ^{1}H NMR spectrum of **3b** in MeOH-d_4.

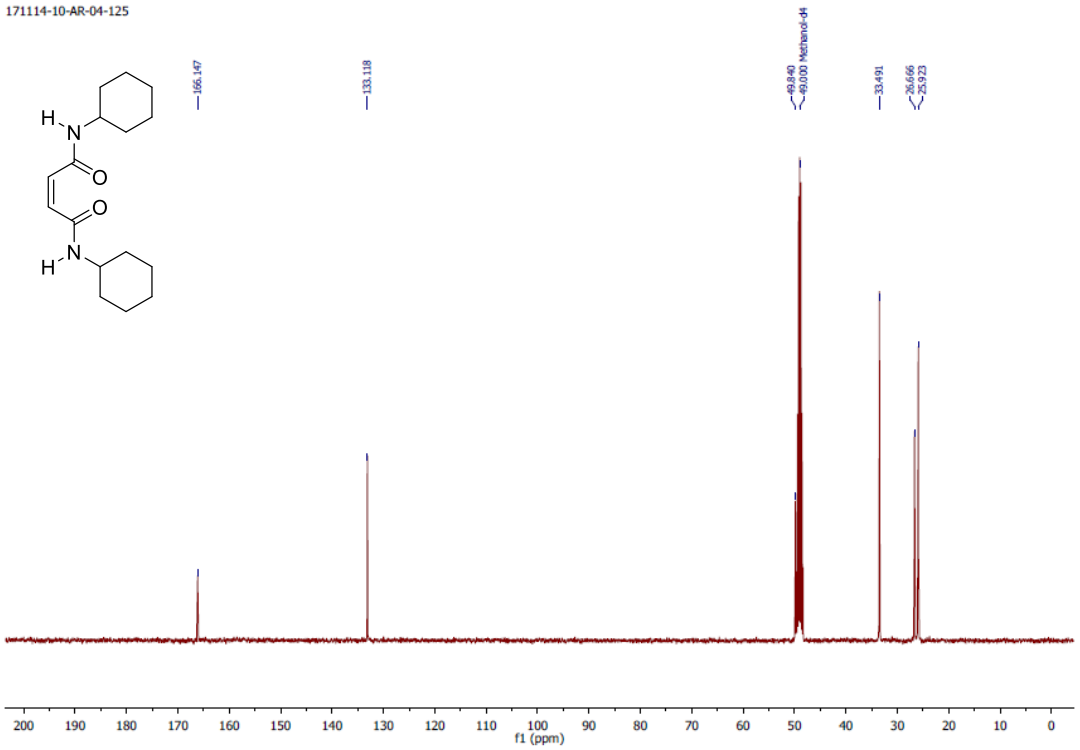

Fig. S40 ^{13}C NMR spectrum of **3b** in MeOH-d_4.

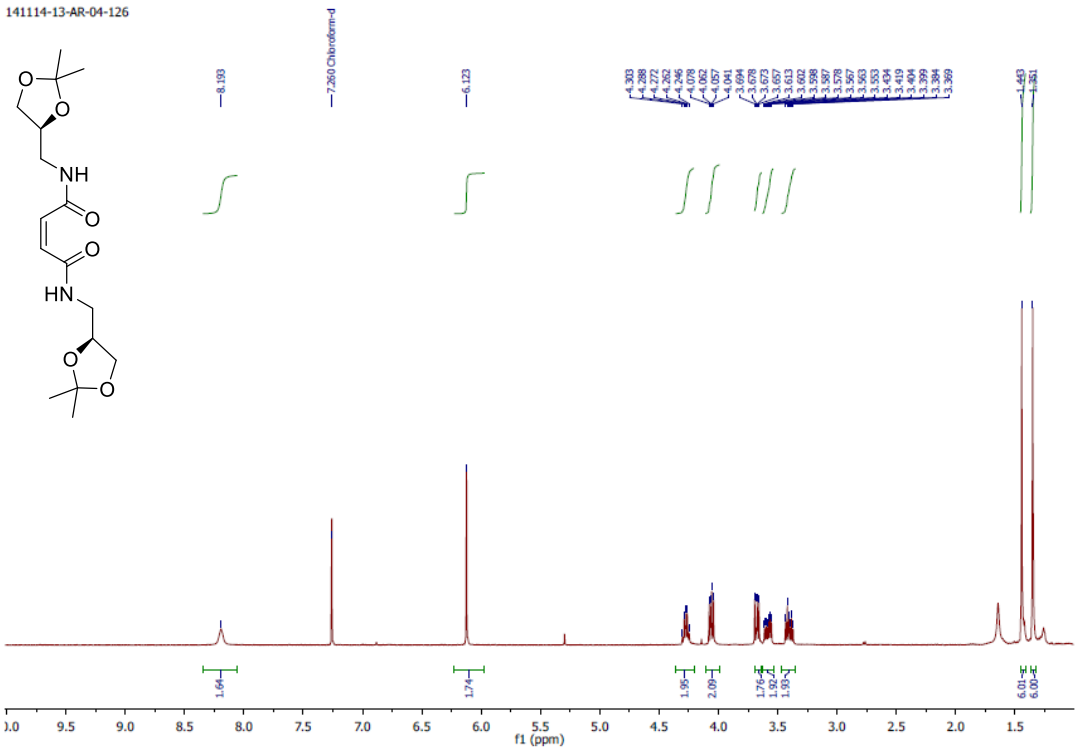

Fig. S41 ^{1}H NMR spectrum of **4b** in $CDCl_3$.

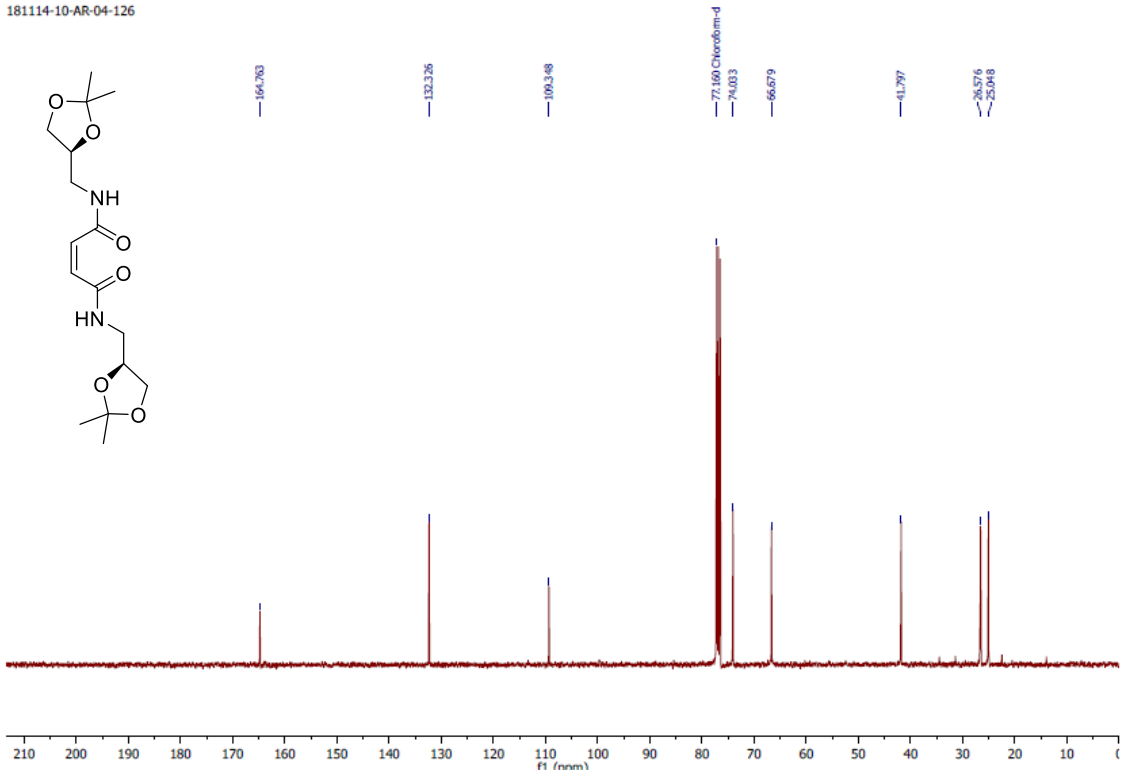

Fig. S42 ^{13}C NMR spectrum of **4b** in $CDCl_3$.

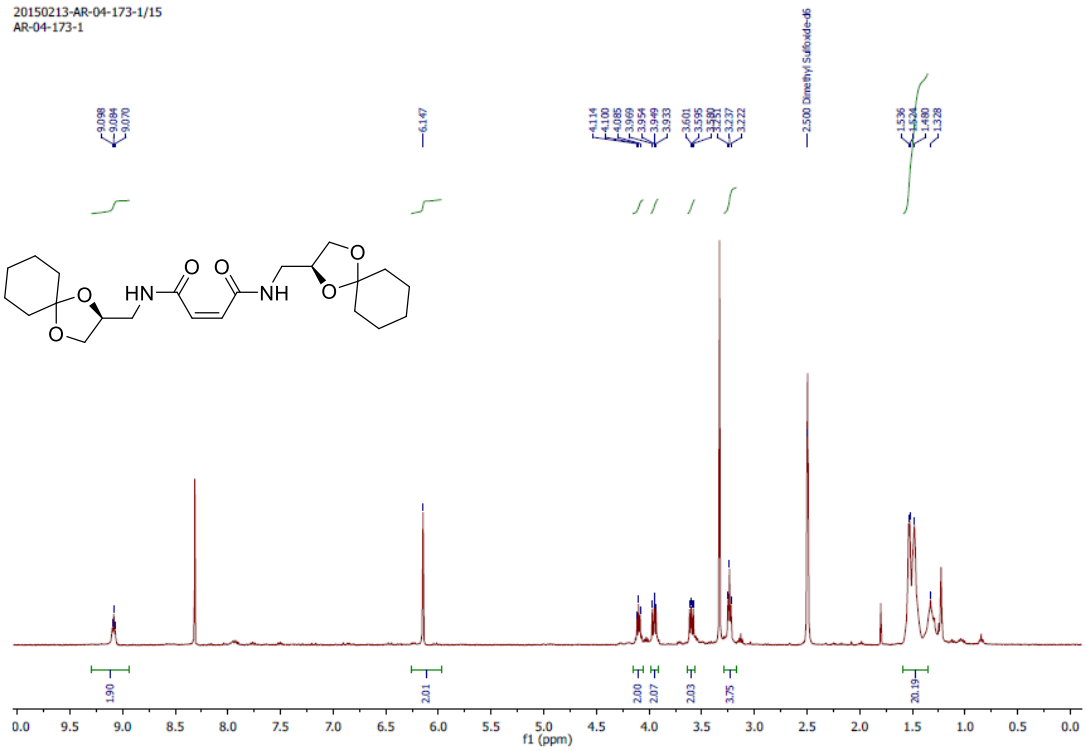

Fig. S43 ^{1}H NMR spectrum of **5b** in DMSO-d_6.

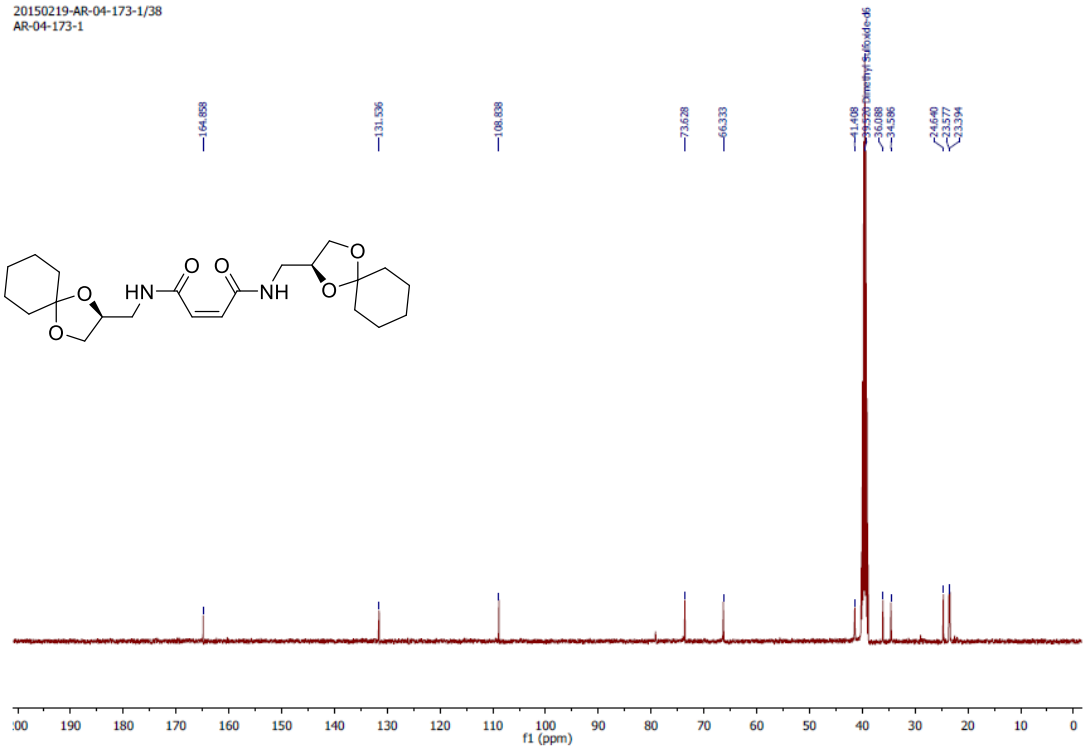

Fig. S44 ^{13}C NMR spectrum of **5b** in DMSO-d_6.

IX. References

S1. A. Chattopadhyay and V. R. Mamdapur, *J. Org. Chem*., 1995, **60**, 585.
S2. A. Rouf, M. A. Aga, B. Kumar and S. C. Taneja, *Tetrahedron Lett.*, 2013, **54**, 6420.
S3. S. K. Chattopadhyay, T. Biswas and T. Biswas, *Tetrahedron Lett.*, 2008, **49**, 1365.
S4. T. J. Baker and M. Goodman, *Synthesis*, 1999, **1999**, 1423.
S5. N. B. Mehta, A. P. Phillips, F. F. Lui and R. E. Brooks, *J. Org. Chem.*, 1960, **25**, 1012.
S6. J. Streuff and K. Muñiz, *J. Organomet. Chem.,* 2005, **690**, 5973.
S7. B. B. Lohray, A. Sekar Reddy and V. Bhushan, *Tetrahedron: Asymmetry*, 1996, **7**, 2411.
S8. P. Saisaha, D. Pijper, R. P. van Summeren, R. Hoen, C. Smit, J. W. de Boer, R. Hage, P. L. Alsters, B. L. Feringa and W. R. Browne, *Org. Biomol. Chem.*, 2010, **8**, 4444.
S9. A. Roy, D. Saha, A. Mukherjee and P. Talukdar, *Organic Lett.*, 2016, **18**, 5864.
S10. A. Roy, D. Saha, P. S. Mandal, A. Mukherjee and P. Talukdar, *Chem. Eur. J.*, 2016, **23**, 1241.
S11. A. Roy, T. Saha, M. L. Gening, D. V. Titov, A. G. Gerbst, Y. E. Tsvetkov, N. E. Nifantiev and P. Talukdar, *Chem. Eur. J.*, 2015, **21**, 17445.
S12. A. V. Jentzsch, D. Emery, J. Mareda, S. K. Nayak, P. Metrangolo, G. Resnati, N. Sakai and S. Matile, *Nat. Commun.*, 2012, **3**, 905.
S13. S. P. Meisburger, W. C. Thomas, M. B. Watkins and N. Ando, *Chem. Rev.*, 2017, **117**, 7615.
S14. F. Biscarini, M. Cavallini, D. A. Leigh, S. León, S. J. Teat, J. K. Y. Wong and F. Zerbetto, *J. Am. Chem. Soc.*, 2002, **124**, 225.
S15. P. W. Baures, A. M. Beatty, M. Dhanasekaran, B. A. Helfrich, W. Pérez-Segarra and J. Desper, *J. Am. Chem. Soc.*, 2002, **124**, 11315.
S16. B. T. Gowda, S. Foro, K. Shakuntala and H. Fuess, *Acta Crystallogr. E*, 2011, **67**, o117.
S17. K. Shakuntala, S. Foro and B. T. Gowda, *Acta Crystallogr. E*, 2011, **67**, o1415.
S18. (a) SAINT Plus, (Version 7.03); Bruker AXS Inc.: Madison, WI, 2004; (b) G. M. Sheldrick, SHELXTL, Reference Manual: version 5.1: Bruker AXS; Madison, WI, 1997; (c) G. M. Sheldrick, Acta Crystallogr. Sect. A, 2008, 112; (d) WINGX version 1.80.05 Louis Farrugia, University of Glasgow; (e) A. L. Spek, A PLATON, Multipurpose Crystallographic Tool, Utrecht University, Utrecht, The Netherlands, 2005.
S19. J. J. P. Stewart, *MOPAC2012*, Stewart Computational Chemistry, Colorado Springs, CO, USA, 2012.
S20. M. Korth, *J. Chem. Theory Comput.*, 2010, **6**, 3808.